

ARISTOTLE UNIVERSITY OF THESSALONIKI

**The M/L ratio of clusters and Ω_m
parameter**

by

Alexandros Papastergiou

A thesis submitted in partial fulfillment for the
degree of BSc in Physics

in the
Faculty of Physics
Department of Science

February 2015

Declaration of Authorship

I, Alexandros Papastergiou, declare that this thesis titled, ‘The M/L ratio of Clusters and Ω_m Parameter’ and the work presented in it are my own. I confirm that:

- This work was done wholly or mainly while in candidature for a research degree at this University.
- Where any part of this thesis has previously been submitted for a degree or any other qualification at this University or any other institution, this has been clearly stated.
- Where I have consulted the published work of others, this is always clearly attributed.
- Where I have quoted from the work of others, the source is always given. With the exception of such quotations, this thesis is entirely my own work.
- I have acknowledged all main sources of help.
- Where the thesis is based on work done by myself jointly with others, I have made clear exactly what was done by others and what I have contributed myself.

Signed:

Date:

"Everything existing in the universe is the fruit of chance and necessity."

Democritus

ARISTOTLE UNIVERSITY OF THESSALONIKI

Abstract

Faculty of Physics
Department of Science

by [Alexandros Papastergiou](#)

In this thesis, we estimate for a sample of Abell clusters of galaxies their dynamical masses and their galaxy luminosity functions, using data of the SDSS spectroscopic survey. We first estimate the redshift distribution of galaxies in the region of the cluster and fit gaussians onto them. We then clip the cluster velocity dispersions to a 3σ limit, which is essential to exclude possible outliers, and then estimate the cluster dynamical masses. The masses are found in the 10^{13} - $10^{14} h_{72}^{-1} M_{\odot}$ range, which is perfectly compatible with other works in this field. We also calculate the uncertainties for all the above mentioned parameters using error propagation. We confirm that the derived cluster masses correlate strongly with the number of member galaxies as they should. We then fit a Schechter function to the magnitude distribution of the galaxy members by considering a fixed value of the slope, $\alpha = -1.25$, and find the best-fit values of the main parameters of the function, ie., M_* and ϕ_* . We then estimate the value of the total luminosity of each cluster, as the integral of the first moment of the luminosity function. Through M_* , we also estimate the value of L_* , which is necessary to find the total cluster luminosity, L_{cluster} . Having L_{cluster} we can now easily calculate the M/L ratios of all the clusters in our sample and assuming that the mean cluster M/L ratio is related to its universal value, we can get an estimate of the cosmological density parameter, Ω_m . We finally obtain $\Omega_m \simeq 0.27$ and $\simeq 0.38$, for two different estimates for the cluster M/L value, in good agreement with the values provided by a large number of alternative cosmological probes.

Acknowledgements

I would like to thank my family for their continuous support and patience. I would also like to thank professor Manolis Plionis for accepting to be my supervisor and for providing me with every information and advice I ever needed to complete this thesis.

Contents

Declaration of Authorship	i
Abstract	iii
Acknowledgements	iv
List of Figures	vii
List of Tables	viii
Physical Constants	ix
1 Introduction	1
1.1 General Information on Clusters	1
1.2 Cluster Formation	3
1.3 Types of Clusters	4
1.3.1 Clusters by appearance	4
1.3.2 Clusters by richness	5
1.4 Cluster Masses	6
1.4.1 Methods of estimation and comparison	6
1.4.2 Virial Theorem mass estimates	7
1.4.3 X-ray observation mass estimates	8
1.4.4 Gravitational Lensing	8
1.4.5 Comparing X-ray observation and Gravitational Lensing	9
1.4.6 Sunyaev-Zel'dovich Effect	10
1.5 Luminosity Function of Clusters	10
2 Observational Data	13
2.1 The cluster sample and its basic properties	13
2.2 Visualisation of the Clusters	15
2.3 Cluster Velocity Dispersions	17
3 Cluster Dynamical Analysis and the value of Ω_m	20
3.1 Cluster Masses and Radii	20
3.2 Luminosity Function analysis	22

3.3	Correlations between Mass and Richness	23
3.4	Cluster M/L Ratios & Ω_m	27
3.5	Cluster M/L Ratio Analysis	27
4	Conclusions	31
4.1	Overview of the thesis work	31
4.2	Future research	32
A	Equal Area Projection Diagrams	34
B	Velocity Dispersion Diagrams	41
C	Luminosity Function Diagrams	48
	Bibliography	53

List of Figures

1.1	The Perseus Galaxy Cluster, one of the most impressive clusters observed.	2
1.2	Left Panel : Coma Cluster (regular cluster) , Right Panel : Fornax Cluster (irregular cluster)	4
1.3	Left Panel : Pandora Cluster (rich cluster) , Right Panel : Hercules Cluster (poor cluster)	6
1.4	The gravitational lensing effect as observed at A2218 cluster.	9
1.5	The r-band SDSS DR6 Luminosity Function. Best-fit values of the Schechter parameters α , M_* and ϕ_* are also shown.	12
2.1	Equal area projections, from top-left to bottom-right, of the clusters: A85, A1213, A1656, A1795, A1983 and A2199 clusters.	16
2.2	From top left to bottom right : Cluster velocity dispersion diagrams and gaussian fits for clusters : A85,A1213, A1656, A1795,A1983,A2199.	18
3.1	From top left to bottom right: Galaxy luminosity functions of the clusters A85, A1213, A1656, A1795, A1983 and A2199.	25
3.2	Left Panel: Dynamical mass versus number of bright cluster member galaxies. Right Panel: Dynamical mass versus Abell richness classes, for the clusters of our sample.	26
3.3	Mass to M/L diagram.	29

List of Tables

2.1	Initial Cluster Data	14
2.2	Definition of Abell's Richness Class.	14
2.3	Cluster velocity dispersions and errors	19
3.1	Cluster Radii, Masses and their uncertainties	21
3.2	Best-fit Schechter luminosity function parameters and χ^2/dof values.	24
3.3	Correlation coefficients for N-M and N-R.	27
3.4	Cluster M/L Ratios and uncertainties.	28

Physical Constants

Speed of Light	c	$=$	$2.997 \times 10^8 \text{ m s}^{-2}$
Gravitational Constant	G	$=$	$4.302 \times 10^{-3} pc(km/s)^2 M_{\odot}^{-1}$
Hubble Constant	H_0	$=$	$72 \times kms^{-1} Mpc^{-1}$

Dedicated to my family.

Chapter 1

Introduction

1.1 General Information on Clusters

It is necessary to first give a small introduction on the definition of clusters. A cluster, is a group of galaxies (containing either hundreds or thousands of galaxies), gravitationally bound together. Studying the distribution of galaxies on the sky, we can easily verify that most of them tend to concentrate and create such groups.

Clusters were considered the biggest structures to be found in the entire universe, until the discovery of superclusters. Also, they are the most virialized systems we know of and they can provide us with great information on galaxy formation and cosmology (Bahcall, 1996).

Clustering in the Universe can be detected on many different scales, from poor groups of galaxies, to rich clusters and finally superclusters. In general, clusters span around at an area of $1-3 h^{-1}$ Mpc, and contain hundreds of galaxies in their core region. Their density is also typically a lot bigger than the universal mean density. In any case though, ranging from 10^{14} - $10^{15} h^{-1} M_{\odot}$, clusters are the largest gravitationally bound systems, bearing also a dynamical equilibrium.

Although clusters consist of a great number of galaxies, those galaxies only make up for a minor percentage of the cluster's mass. Most of the mass comes in the form of dark matter and baryons of the hot intracluster gas.

Depending on the number of galaxies they consist of, clusters are categorized as either poor (few galaxies) or rich (many hundreds of galaxies). According to the Abell criterion (Abell,1958), a cluster needs to have at least 30 galaxies in the interval between m_3 and m_3+2 (where m_3 is the magnitude of the third brightest cluster member) to be considered



FIGURE 1.1: The Perseus Galaxy Cluster, one of the most impressive clusters observed.

as rich. The poor ones, tend to present irregularities in their shape, something that is not the case for the rich ones.

Except for galaxies, clusters also contain intracluster gas, dark matter and radio plasmas. Frankly, the optically visible part of a cluster is way less than its "invisible" (to the eye) counterparts. More precisely, all the visible galaxies added, make up for less than 5% of the cluster's mass. On the other hand, the intracluster medium accounts for about 9-10% of the mass, with dark matter being the primary ingredient, with a percentage reaching about 85%.

It is obvious therefore, that if someone is to add up the masses of all the luminous contents of a cluster, he would never get a value for its total mass even remotely close to the real one.

The only largest than clusters structure ever observed, are the superclusters, which span across regions of around $10\text{-}30 h^{-1} \text{ Mpc}$ and have a mass of $\approx 10^{16} h^{-1} M_{\odot}$ and consisting of several clusters together. The difference of course is that they are not gravitationally bound and in a dynamic equilibrium, as there is not enough time for them to reach such a state of evolution.

Groups of galaxies hold the key to unlocking a lot of the Universe's secrets, especially when it comes to issues such as Dark Matter. After all, clusters have always fascinated astronomers, as they are nature's laboratories for testing models of gravitational

structure formation, galaxy evolution, thermodynamics of the intergalactic medium and plasma physics.

Furthermore, spectroscopic observations of clusters is another very direct way of unveiling the procedures that took part after the Big Bang which led to the current distribution of matter. These are, in place, the topics that are mainly going to be extensively described in this first introductory chapter.

1.2 Cluster Formation

The first major topic that needs to be described and explained, is galaxy cluster formation. This is a subject that has been studied for decades, until establishing the current existing model.

Initially, galaxy clusters, were thought to be dynamically relaxed systems, evolving slowly after an initial short-lived episode of violent relaxation. Observations, though, showed that almost half of the rich clusters contain significant substructures (or subgroups), with complex gravitational potentials (eg. Forman et al. 2002).

This was a very interesting discovery, because it proved that clusters are undergoing mergers even at the present day. Obviously, that means that they are not completely relaxed systems, as previously thought, and that cluster formation continues happening even at our era (Jones et al. 2008)

The current theory explaining how clusters form and evolve is called hierarchical clustering. In general, hierarchical clustering is a term referring to the process by which larger structures are formed through the continuous merging of smaller ones. We can easily include the formation of a cluster in the spectrum of phenomena described by hierarchical clustering. Initially, the formation is triggered by the collapse of the largest overdensities in the density field, which are however of small size. That is to say, everything starts with small scale instabilities. Those small scale instabilities get easily amplified (gravitationally) and take part in the creation of clusters through infall of matter and merger of small subgroups or subclusters along anisotropic large scale structures (filaments) (eg. Jones et al. 2008).

Specifically, on large scales, filaments containing gas and galaxies form around voids, with clusters forming at the intersection of these filaments which then grow through the accretion of matter and groups which move along the filament and fall into the cluster potential (Jones et al. 2008).

The mergers of large subgroups that take part in the process of cluster formation are the most energetic phenomena in the Universe, with energies up to 10^{64} ergs.

When subclusters collide (merge) to form a cluster, the energy of the gas contained in both clusters is mainly transformed into thermal energy by shocks and turbulence, whilst some small-scale events such as amplification of the magnetic field and inverse Compton radiation also appear.

Finally, because clusters are formed through hierarchical clustering and are the largest bound systems in the Universe, they always trace back to the initial conditions of their formation. This characteristic is very important, as it proves that there is a strong dependence between the cosmological parameters of the Universe and the way these structures evolved. For this reason exactly, in this thesis, we will estimate the value of the cosmological density Ω_m parameter, through calculations of the mass and luminosity of our sample of clusters (eg. Bahcall,1996).

All the above processes taking place during a cluster's formation, prove that clusters are nature's best laboratories for testing models of gravitational structure formation, galaxy evolution, thermodynamics of the intergalactic medium and plasma physics as well as a plethora of other fascinating oricesses. (Kravtsov et al. 2012).

1.3 Types of Clusters

1.3.1 Clusters by appearance



FIGURE 1.2: Left Panel : Coma Cluster (regular cluster) , Right Panel : Fornax Cluster (irregular cluster)

There are several classifications of clusters depending on many of their individual characteristics, like shape, richness, galaxy content, etc. In this section, we will focus on the classification having to do with their shape. There are 2 categories of clusters, based on their appearance :

1. Regular Galaxy Clusters
2. Irregular Galaxy Clusters.

Regular clusters are spherically symmetric, with the galaxies concentrated towards their center. Usually, they contain more than 1000 galaxies which are brighter on average than $M \approx -16$ (Bahcall 1996). The fraction of elliptical to spiral galaxies is significantly larger in such clusters with respect to the field. A typical example of a regular cluster is the Coma Cluster.

Irregular Galaxy Clusters do not have a well-defined center, but are often made up of loose smaller groups of galaxies, called subclusters. They contain all types of galaxies, spirals, irregulars and ellipticals and they can contain from just a few to over 1000 galaxies (Bahcall 1996). Our Local group of galaxies can be characterised as a very poor irregular cluster.

In fig. (1.2) and (1.3) we present the image of a regular and an irregular cluster, in which we can easily observe the regularity (and irregularity respectively) of the cluster's shape.

1.3.2 Clusters by richness

Clusters can also be classified by richness. They, can be divided them into 2 categories:

1. rich clusters
2. poor clusters.

A rich cluster contains hundreds to thousands galaxy members. The largest galaxies are typically found near the cluster center. They contain a higher fraction of elliptical and S0 type of galaxies, with respect to poorer clusters and also contain large quantities of hot intracluster gas. A poor cluster on the other hand, contains only tens to a few hundred of galaxies and usually they have a ragged and irregular appearance and they contain a lot more spiral and irregular galaxies with respect to richer clusters. In the images of figure (1.3), we can see A2744, also called Pandora Cluster, which is a rich cluster containing thousands of galaxies, and also the Hercules cluster, which is particularly poor, with only a few tens of galaxies.



FIGURE 1.3: Left Panel : Pandora Cluster (rich cluster) , Right Panel : Hercules Cluster (poor cluster)

1.4 Cluster Masses

1.4.1 Methods of estimation and comparison

To start with, we must underline that a rich cluster has a mass of around $10^{14}M_{\odot}$ to $10^{15}M_{\odot}$ (Bahcall 1996) . Therefore, they are massive structures and cannot be compared to anything other observed in the Universe, except probably for superclusters, which however are not gravitationally bound objects.

The first astronomer to estimate the masses of Clusters, was Zwicky, whose work revealed the existence of Dark Matter. It was his work that highlighted the fact that estimating a cluster's mass using the emitted light (that is to say galaxies and intracluster gas) does not produce a large enough value, essential to ensure that a cluster would stay gravitationally bound.

The above result, and other similar results from subsequent studies, led to the introduction of the notion of Dark Matter in Cosmology. Since the observed light corresponds to a cluster mass that is significantly less than that needed for the cluster to be gravitationally bound, the required mass is invisible in any part of the electromagnetic spectrum. This mass is what is called Dark Matter, which in fact not only exists in clusters, but in all gravitationally bound cosmic structures.

In this section of the thesis, we will describe the 3 main methods used to measure the mass of a cluster. These are :

- a) Virial Theorem: we can calculate the mass using the cluster velocity dispersion, assuming that the clusters obey the hydrostatic equilibrium (which is the method we will use in this Thesis).
- b) Euler's equation: using the X-ray emitting gas as a trace of the total cluster potential.
- c) Gravitational Lensing: by observing the distortions of the background galaxy images due to gravity, we can estimate the mass of a cluster. This is the most widespread and used method in the recent times (Mahdavi et al. 2007).

It is worth noting, that the results obtained from each of these 3 methods are consistent with each other, which guarantees that they can all be used quite effectively for our calculations. Of course, not all methods are equally accurate, nor equally easy to apply to any given cluster. Still, we will highlight some key aspects of each method (Bahcall 1996, Xiang-Ping Wu et al. 1997)

1.4.2 Virial Theorem mass estimates

This is the simplest and most straightforward method to estimate a cluster's mass, but at the the same time it is the one requiring most assumptions and simplifications. At first we certainly have to assume that a cluster is in dynamical equilibrium. Then through the Virial theorem we deduce the relation between the total mass, the size and the velocity dispersion, according to Borgani:

$$M = \frac{3}{2} \frac{\pi v_d^2 R_v}{G}. \quad (1.1)$$

Estimating observationally the Virial Radius, R_v and the velocity dispersion along the line-of-sight, v_d , we can easily obtain an arithmetic value for the mass of a cluster.

There are of course some disadvantages when using this method. For example, it is difficult to "decontaminate" the cluster of any non-member galaxies. There is always a risk that we might include galaxies that belong either in the background or the foreground of the cluster.

Another setback, which is probably even more important, is the fact that when we use the Virial Theorem, we assume that the Dark Matter distribution, follows that of the light distribution. To this day, there is still no proof or knowledge on the relation between the two distributions. If the dark matter is more concentrated than the light we are bound to overestimate its mass, whilst if it is less concentrated we will underestimate it (Sadat 1995).

Even with these disadvantages though, this method can provide satisfactory results.

1.4.3 X-ray observation mass estimates

Galaxy clusters contain a lot of hot ionized gas. Intracluster gas is the main component of baryonic matter in the clusters. It represents a large fraction of the total cluster mass, up to 30% of it. This hot gas emits high energy photons in the form of thermal bremsstrahlung. Using this radiation, we can estimate the temperature of the gas and through Euler's equation we can obtain an arithmetic value for the mass of the whole cluster as well. To deduce the mass from the temperature of the gas, we assume once more hydrostatic equilibrium.

There are plenty of advantages in using this particular method. We do not need to determine which of the galaxies really belong to the cluster, because it doesn't affect this calculation. Also, there is no need to make any assumptions about the Dark Matter distribution, as in the dynamical estimation. The setback in using this method, is that it is cumbersome to obtain the data required from the clusters, through X-ray imaging, while assuming hydrostatic equilibrium is again not an accurate assumption to make when examining a cluster that is still in the process of merging or forming.

1.4.4 Gravitational Lensing

Gravitational Lensing is a very powerful tool to directly measure the projected cluster mass distribution. When light passes near a cluster, the cluster's gravity causes the light to bend slightly from its initial path. As a result, the shape of galaxies behind the cluster and along our line of sight appear slightly distorted on the sky. By measuring the average shape change of background galaxies in different areas around the cluster, we can estimate its surface mass profile.

At this point, we have to note that there are two kinds of gravitational lensing, the weak and the strong lensing. The strong lensing, is mostly used for observations around the central area of the cluster. More specifically it refers to a method used to calculate the mass of the cluster that is contained within the "Einstein Radius". The distortion appears in the form of strong arcs observed around the core of the cluster. The weak lensing on the other hand is used mostly to estimate the mass observed in the outer regions of the cluster. Technically, it is also based on the same assumptions as the strong lensing. What makes both of them very useful techniques is the fact that they can be based on data in the visible (or near infrared) band and do not require data from

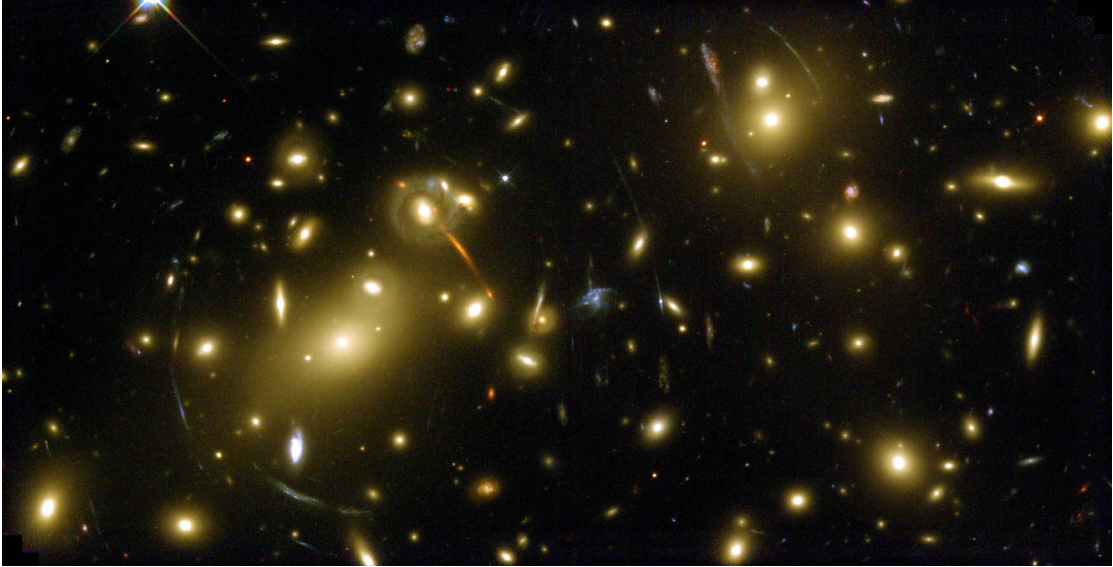


FIGURE 1.4: The gravitational lensing effect as observed at A2218 cluster.

many areas of the spectrum. The cluster of fig (1.6) (A2218) shows clearly the distortion of galaxies and structures due to weak and strong lensing.

1.4.5 Comparing X-ray observation and Gravitational Lensing

An interesting conclusion arises if we compare the X-ray estimate with those of Gravitational Lensing. It has been noted that there is a difference in the mass calculated by the two methods, around the central areas of the cluster. The results systematically showed a difference of a factor of around 2-2.5 between the X-ray observation and the strong Lensing (Sadat 1995, Mahdavi et al. 2008).

At larger radii, the difference seems to increase, while near the center both the weak lensing and X-ray observations provide the same results. Therefore, the difference of the two techniques is restricted mostly to the central areas (Sadat 1995, Mahdavi et al. 2008).

There are several factors as to why these methods might disagree. In general, the fact that X-ray estimates differ from lensing at large radii, may occur due to the hydrostatic equilibrium assumption being invalid, due to merging effects, instability of the equilibrium equation or non-thermal pressure. Unfortunately it is not clear yet to tell which one of these effects mostly creates the differences in the mass measurements.

1.4.6 Sunyaev-Zel'dovich Effect

Although not mentioned above, among the primary methods of estimating a cluster's mass, this is a recent and interesting method.

To start with, the Sunyaev-Zel'dovich Effect is the distortion of the Cosmic Microwave Background (CMB) by high energy electrons through inverse Compton scattering. As a CMB photon passes through a cluster it interacts with high energy electrons contained in the intracluster hot gas (Bahcall 1996). The result of this interaction is that it slightly heats the CMB in the direction of the cluster. So, the presence of a cluster creates a "signature" in the cosmic microwave background, which would not be seen otherwise.

It can be shown that this change in the cosmic microwave background only depends on the cluster's mass. Measuring then the change a cluster induces to the CMB, we can analytically calculate the mass needed to justify such a measurement.

What is really interesting about this effect is that it is totally independent of a cluster's redshift and for as long as there are regions with large electron pressures, the Sunyaev-Zel'dovich Effect should be detectable and able to give us results, no matter how far away in the Universe we observe.

1.5 Luminosity Function of Clusters

A very important tool (largely discussed also in this paper) to study the characteristics of a cluster is the luminosity function (L.F) of its galaxy members. Luminosity functions are used mostly to study the luminosity distribution of large groups of galaxies or other sources of electromagnetic radiation. By definition, a luminosity function is the number density of sources in luminosity intervals. An important mathematical parametrisation of the luminosity function which is analytic, continuous and has interesting mathematical procedures, was found by Schechter in 1976 and thus it is since called the Schechter luminosity function.

There are 2 major reasons as to why we need to study the Luminosity function of a cluster. First, to compare the luminosity functions of galaxies inside a cluster to those of field galaxies, thus understanding the influence of environment on the global statistical properties of galaxies. Secondly, to compare luminosity functions of different clusters, in an effort to understand if there have been differences in the galaxy formation processes, due to different environments (Popesso et al.,2005)

The luminosity function of a cluster provides important information on the :

- primordial density fluctuations
- processes that destroy or create new galaxies
- processes that change one galaxy type into another
- processes that transform mass into light.

As already mentioned, a luminosity function is best fitted by a function called Schechter function. The advantages of this function are that it is analytic, continuous and that it has interesting mathematical procedures. The formula describing the Schechter function in terms of luminosities is (Schechter 1976):

$$\Phi(L) = \phi_* \left(\frac{L}{L_*} \right)^\alpha \exp -\frac{L}{L_*} \quad (1.2)$$

which in terms of magnitudes can be written as:

$$\Phi(M) = 0.4 \log(10) \phi_* 10^{-0.4(M-M_*)(\alpha+1)} \exp \left[-10^{-0.4(M-M_*)} \right] \quad (1.3)$$

where L_* (or M_*) is the luminosity (or absolute magnitude) that separates the low and the high luminosity (or magnitude) parts, and ϕ_* is a normalisation constant for the function with units of density.

As it is easy to see from the above formula, at luminosities $L < L_*$ the power law part of $\Phi(L)$ dominates, whilst at magnitudes $L > L_*$ the exponential cutoff dominates. Therefore, most of the galaxies occupy the first part of the luminosity distribution, while very few the most luminous, the second part of $\Phi(L)$.

From the definition of the luminosity function, it is easy to see that the mean density of galaxies down to a particular luminosity limit is given by integrating the luminosity function:

$$\langle n \rangle = \int_{L_{\min}}^{\infty} \Phi(L) dL = L_* \int_{L_{\min}/L_*}^{\infty} \Phi \left(\frac{L}{L_*} \right) d \left(\frac{L}{L_*} \right) \quad (1.4)$$

while the mean luminosity density is similarly given by:

$$\langle L \rangle = \int_{L_{\min}}^{\infty} L \Phi(L) dL = L_*^2 \int_{L_{\min}/L_*}^{\infty} \frac{L}{L_*} \Phi \left(\frac{L}{L_*} \right) d \left(\frac{L}{L_*} \right) \quad (1.5)$$

Due to the analytical form of the Schether function, it is easy to show that:

$$\langle n \rangle = \phi_* \Gamma' \left(\alpha + 1, \frac{L_{\min}}{L_*} \right) \quad (1.6)$$

and

$$\langle L \rangle = \phi_* L_* \Gamma' \left(\alpha + 2, \frac{L_{\min}}{L_*} \right) \quad (1.7)$$

where Γ' is the incomplete gamma function.

Finally, we present a typical galaxy luminosity function, based on the SDSS data, as estimated by Montero-Dorta et al.(2008).

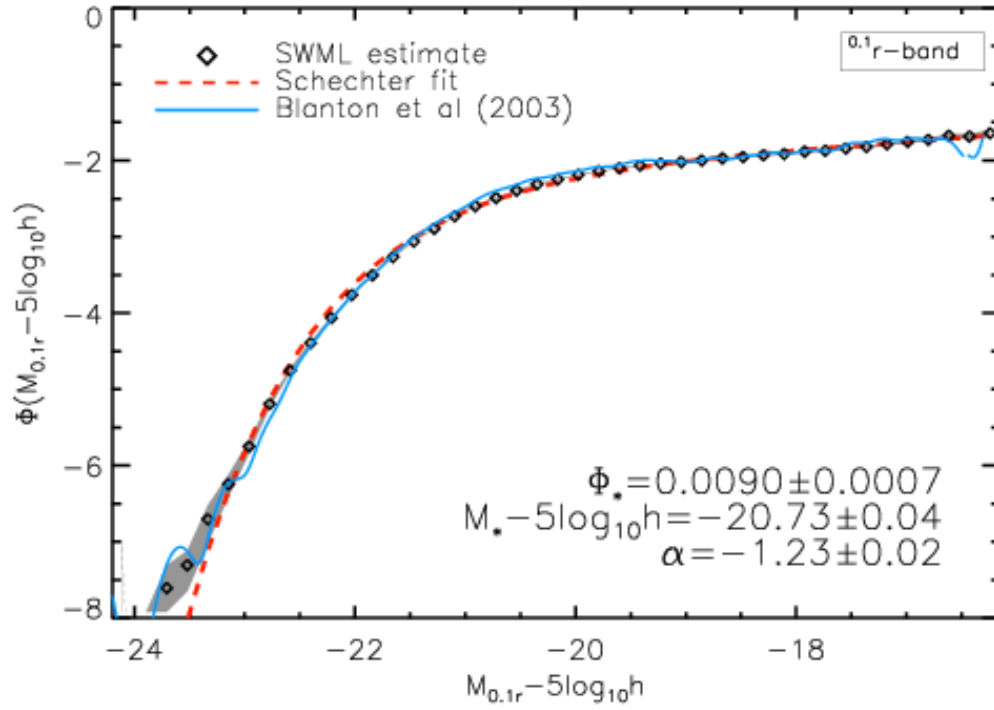


FIGURE 1.5: The r-band SDSS DR6 Luminosity Function. Best-fit values of the Schechter parameters α , M_* and ϕ_* are also shown.

Chapter 2

Observational Data

2.1 The cluster sample and its basic properties

We select a subsample of the Abell (1958, ACO 1989) cluster catalogue such that it samples a wide range of Bautz-Morgan (hereafter BM) types, which correspond to different cluster dynamical states. In total we have 34 such clusters which can be found in the table (2.1), where we list the Abell cluster number, the cluster redshift, its celestial coordinates (α, δ) , the cluster angular diameter distance, d_A , and its Abell richness class, R , which categorises clusters depending on how many galaxies they contain with a magnitude between that of its third brightest member (m_3) and m_3+2 . The different richness categories are provided in table (2.2). Note that the angular diameter distance is given by:

$$d_A = (1+z) \int_0^z \frac{c}{H(z)} dz \quad (2.1)$$

where c is the velocity of light and $H(z)$ is the Hubble function, derived from the first Friedmann's equation, and given by:

$$H(z) = H_0 [\Omega_m(1+z)^3 + \Omega_\Lambda]^{1/2} \quad (2.2)$$

where H_0 is the Hubble constant, which through out this thesis we use $H_0 = 72 \text{ km s}^{-1} \text{ Mpc}^{-1}$, Ω_m is the cosmological matter density parameter and Ω_Λ is the density parameter corresponding to the Cosmological Constant. We also assume through out this thesis a flat Universe, ie., one with $\Omega_m + \Omega_\Lambda = 1$, consistent with the most recent cosmological results (eg., Planck Collaboration results of Ade et al. 2014)

We then identify the galaxy members of these clusters by using the SDSS spectroscopy galaxy catalogue (DR7 revision). The SDSS provides an interface through which one can

TABLE 2.1: Initial Cluster Data

Name	z	α (deg)	δ (deg)	d_A (h_{72}^{-1} Mpc)	R
A85	0.055	10.407	-9.342	243.020	1
A168	0.045	18.790	0.247	193.823	1
A279	0.079	29.092	1.060	353.117	1
A671	0.050	127.122	30.416	218.316	1
A690	0.078	129.809	28.840	348.494	1
A957	0.043	153.488	-0.915	189.31	1
A971	0.092	154.944	40.965	414.24	1
A1177	0.031	167.365	21.695	136.47	0
A1213	0.046	169.121	29.260	202.71	1
A1291	0.052	173.041	56.030	229.54	1
A1468	0.084	181.408	51.421	374.21	1
A1516	0.076	184.738	5.239	339.23	1
A1569	0.073	189.077	16.591	323.06	0
1650	0.083	194.692	-1.753	371.84	2
A1656	0.023	194.952	27.980	99.59	2
A1691	0.072	197.846	39.201	318.32	1
A1738	0.115	201.296	57.600	522.23	2
A1795	0.062	207.252	26.585	272.59	2
A1800	0.075	207.422	28.068	332.31	0
A1913	0.052	216.715	16.676	229.56	1
A1983	0.043	223.183	16.746	189.31	1
A1991	0.058	223.625	18.630	256.62	1
A2029	0.077	227.733	5.744	341.52	2
A2079	0.068	232.019	28.877	302.32	1
A2089	0.073	233.172	28.015	322.95	1
A2107	0.041	234.912	21.783	178.23	1
A2124	0.065	236.247	36.061	288.47	1
A2147	0.035	240.571	15.895	149.65	1
A2199	0.030	247.160	39.551	129.94	2
A2244	0.096	255.683	34.046	433.19	2
A2255	0.080	258.129	64.092	357.74	2
A2356	0.116	323.942	0.115	526.96	2
A2399	0.057	329.385	-7.794	252.14	1
A2428	0.085	334.061	-9.350	378.79	1
A2593	0.041	351.129	14.641	178.26	0
A2670	0.076	358.557	-10.418	336.85	3

TABLE 2.2: Definition of Abell's Richness Class.

Richness class	Number of galaxy counts
Group 0	30-49
Group 1	50-79
Group 2	80-129
Group 3	130-199
Group 4	200-299
Group 5	more than 299

select the area of the sky in which he/she is interested in and download the spectroscopic data available.

We select as members of each cluster those galaxies that fulfill a range of criteria. These criteria are:

- Candidate galaxy members are selected within a $1.5 h^{-1}$ Mpc distance from the cluster center. To this end we transform this radius in the corresponding angular separation by:

$$\theta = \arctan\left(\frac{1.5}{d_A}\right) = \frac{1.5}{d_A} \text{ radians} \quad (2.3)$$

- Candidate galaxy members are selected within a specific range of radial velocity difference from the cluster center. This is because in a cluster all the members should move at relatively close velocities to each other. Assuming that some galaxies in our area of $1.5 h^{-1}$ Mpc, specified above, are moving at a significantly different speed than they should, we could then easily conclude that they are either background or foreground galaxies. So comes the second condition of our algorithm, which is that we only accept galaxies, within a ± 2000 km/s range of the cluster center velocity. That is a rather large range which will be further reduced, but for the sake of other possible future studies, we will initially allow it.

The above mentioned procedure, is necessary to make sure that we only use galaxies that are specifically cluster members. This is obviously very important, if we want our results to be accurate and "noise-free". A correct initial set of data is the first step towards bias-free results.

2.2 Visualisation of the Clusters

In order to get an idea of the spatial distribution of galaxies within clusters we plot the distribution of galaxy members in an equal area projection. To this end, we use as the x-coordinate of the plot the right ascension of each galaxy member multiplied by the cosine of the declination of the cluster center ($x = \alpha \times \cos(\delta_0)$) and as y-coordinate the galaxy member's declination. These plots provide therefore an idea of the projected shape of the cluster on the plane of the sky. In order to inspect whether galaxies of different luminosities follow the same density profile, since, for example, a very bright galaxy far away from the center would be suspect of being a projection effect. we plot with different colours the galaxies in 3 different magnitude ranges (black, blue and red correspond to the 10% brightest, the 10%-30% less bright and the 30% least bright galaxies, respectively).

Using these diagrams, we can also identify whether a cluster contains subgroups of galaxies, which we then can attempt to study separately. Below we present some examples of equal area projection plots, for some of the most prominent clusters in our sample.

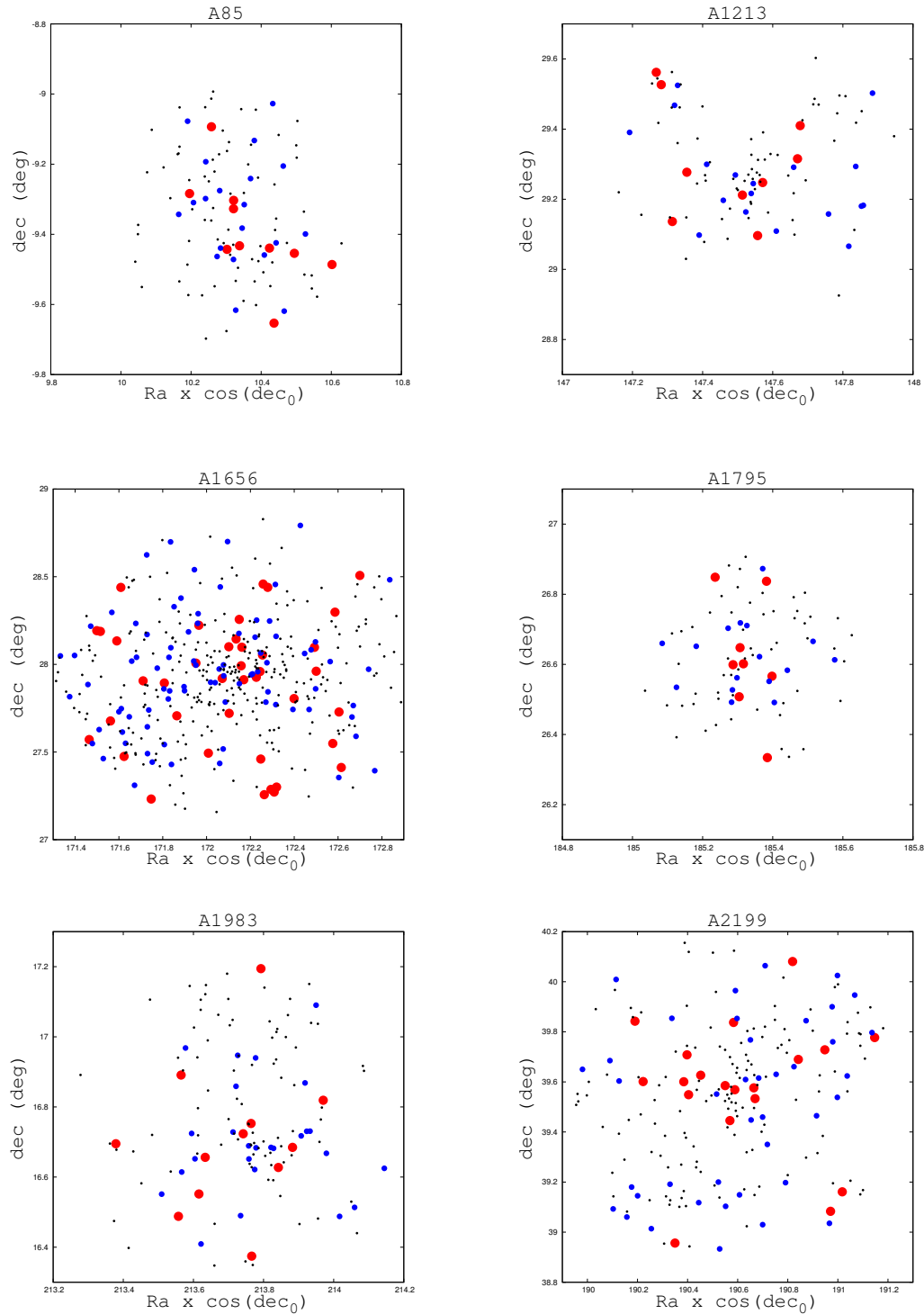


FIGURE 2.1: Equal area projections, from top-left to bottom-right, of the clusters: A85, A1213, A1656, A1795, A1983 and A2199 clusters.

2.3 Cluster Velocity Dispersions

One of the most significant goals of this thesis is to attempt to accurately estimate clusters masses using the virial theorem. To this end it is essential to estimate and use the cluster velocity dispersion for which we use the redshifts of the galaxy members and the corresponding recessional velocities: $v = zc$. Having estimated the velocities of all the galaxy members, we estimate the mean velocity of the entire cluster. We then subtract each galaxy velocity from the mean cluster velocity in order to rest the velocities with respect to the mean cluster one. The cluster velocity dispersion can be estimated according to the formula:

$$v_d = \frac{\sum_i (v_i - v_{mean})^2}{N_g - 1} \quad (2.4)$$

where v_d is the velocity dispersion, v_i is the velocity of the i^{th} galaxy, v_{mean} the mean velocity of the cluster and N_g is the number of galaxy members of the specific cluster. The $N_g - 1$ term in the denominator renders our calculations unbiased.

In order to determine an accurate value of the cluster velocity dispersion, we need to exclude possible outliers and to this effect we follow a procedure by which we first plot the distribution of galaxy member velocities, normalised to that of the cluster center, and then fit a Gaussian to the distribution. To this end we use a χ^2 minimisation procedure by which we estimate the parameters of the Gaussian, which is overlaid on the galaxy velocity distributions. Having calculated the standard deviation (σ), we now exclude from the sample of galaxies those with velocities further than 3σ from the mean value of the cluster. We calculate the new σ and the procedure is iterated until no galaxy is excluded further.

This procedure allowed us to identify that the clusters A168, A671, A1291 and A2147 consist of three separate groups of galaxies, while A1516 consists of two groups. All the cluster velocity histograms and fitted Gaussians are listed in the Appendix. However, we present here some examples of the most interesting clusters (Fig.2.2).

The final results for each cluster of our sample are listed in Table (3.4). We list the mean velocity of the cluster, the cluster velocity dispersion, v_d , and its uncertainty (both arithmetically and as a percentage), σ_{v_d} . Uncertainties in our measured parameters are estimated through out this thesis using error propagation theory. Note that in some cases, when a cluster appears to have distinct subgroups, we divide and analyse separately these subgroups. It appears that such subgroups, on occasions, seem to be moving at different velocities and can therefore be easily separated and treated as independent systems.

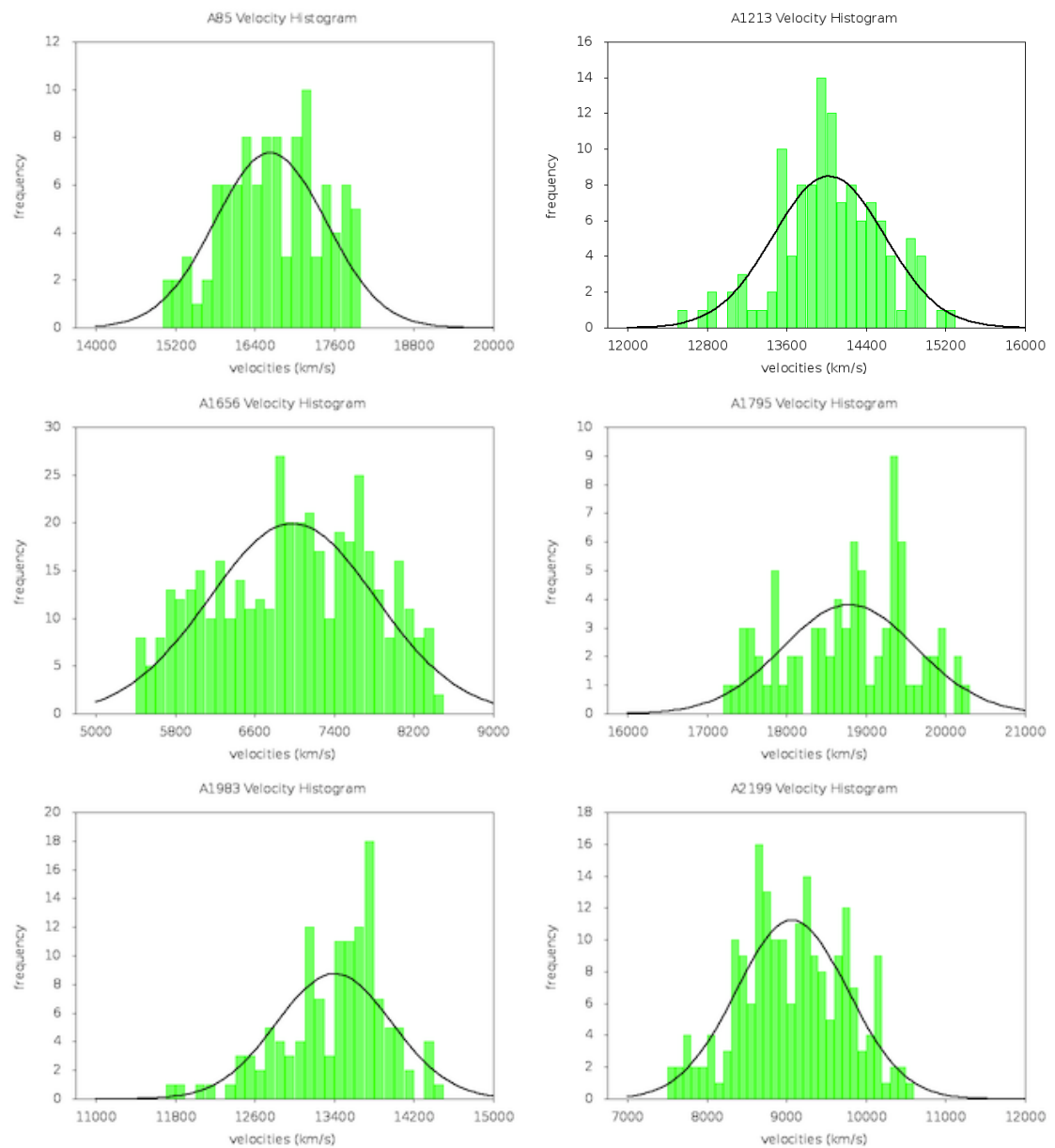


FIGURE 2.2: From top left to bottom right : Cluster velocity dispersion diagrams and gaussian fits for clusters : A85,A1213, A1656, A1795,A1983,A2199.

TABLE 2.3: Cluster velocity dispersions and errors

Name	Mean Velocity (km/s)	v_d (km/s)	σ_{v_d} (km/s)	σ_{v_d} (%)
A85	16693.8	743.9	± 51.8	6.97
A168(1)	12863.9	267.3	± 28.8	10.80
A168(2)	13638.0	243.3	± 20.3	8.35
A168(3)	14406.7	220.8	± 31.1	14.10
A279	23934.7	658.2	± 54.9	8.34
A671(1)	14103.2	253.7	± 30.7	12.10
A671(2)	15088.9	296.3	± 36.1	12.20
A671(3)	16027.7	258.0	± 45.6	17.70
A690	24018.8	480.4	± 60.0	12.50
A957	13328.8	770.8	± 70.1	10.20
A971	27824.3	770.8	± 92.3	11.98
A1177	9630.4	335.7	± 39.9	11.89
A1213	14029.0	616.2	± 35.0	6.70
A1291(1)	14956.5	236.9	± 27.7	11.70
A1291(2)	15719.6	240.6	± 37.7	15.70
A1291(3)	16839.6	259.7	± 44.0	16.97
A1468	25500.2	477.7	± 71.1	14.89
A1516	23183.5	658.7	± 66.6	10.12
A1569	21059.2	444.4	± 72.0	16.21
1650	25100.7	657.1	± 65.6	9.99
A1656	6980.8	775.2	± 25.7	3.32
A1691	21697.9	716.5	± 61.3	8.56
A1738	34898.4	626.1	± 87.0	13.90
A1795	18792.5	777.9	± 70.4	9.05
A1800	22668.7	668.0	± 68.7	10.29
A1913	15896.7	594.4	± 41.1	6.92
A1983	13402.6	526.0	± 33.9	6.45
A1991	17536.5	577.6	± 46.1	7.99
A2029	22082.8	220.6	± 30.0	13.68
A2079	19745.2	365.0	± 35.9	9.84
A2089	22052.6	536.3	± 49.1	9.16
A2107	12389.5	614.7	± 41.3	6.72
A2124	19841.3	741.9	± 61.0	8.23
A2147(1)	9495.9	206.0	± 30.9	15.01
A2147(2)	10783.9	490.9	± 24.6	5.02
A2199	9072.0	663.1	± 33.2	5.01
A2244	29198.6	724.5	± 66.6	9.20
A2255	24081.6	766.4	± 74.1	9.68
A2356	35358.3	509.7	± 74.0	14.52
A2399	17375.6	595.0	± 39.9	6.72
A2428	25217.2	524.7	± 67.6	12.90
A2593	12477.0	624.2	± 49.8	7.98
A2670	22862.9	768.5	± 61.8	8.05

Chapter 3

Cluster Dynamical Analysis and the value of Ω_m

3.1 Cluster Masses and Radii

Assuming dynamical equilibrium and using the Virial Theorem we calculate the virialization Radius and the Cluster Masses in order to complete the dynamic analysis of the clusters. The virial cluster radius is given by (Borgani 2006) :

$$r_v = \frac{N_g(N_g - 1)}{\sum r_{ij}^{-1}} \quad (3.1)$$

where r_{ij} the projected separation of the i, j galaxy pair and $i > j$. Similarly, the virial cluster mass is given by (Borgani 2006; Girardi et al. 1998):

$$M = \frac{3\pi}{2} \frac{r_v v_d^2}{G} (1 - \Delta) \quad (3.2)$$

where v_d is the velocity dispersion, G is the gravitational constant and Δ a fractional correction factor that takes into account the fact that the cluster is not fully enclosed within the sampling radius. This factor depends on the velocity anisotropy of the galaxy orbits (eg., Girardi et al. 1998). We take $\Delta = 0.19$ which is the median value estimated by Girardi et al. (1998).

In Table 3.1 we present the results for all the clusters of our sample and of their subgroups of galaxies. Radii are measured in h_{72}^{-1} Mpc, whilst the masses are calculated in terms of $10^{14} h_{72}^{-1} M_{\odot}$. Uncertainties are estimated using error propagation theory.

We should note here though that the method used to estimate cluster mass is based in a variety of assumptions which render the estimation quite approximate.

TABLE 3.1: Cluster Radii, Masses and their uncertainties

Name	r_v (h_{72}^{-1} Mpc)	Mass ($10^{14}h_{72}^{-1}M_{\odot}$)	σ_M ($10^{14}h_{72}^{-1}M_{\odot}$)
A85	1.54	9.35	± 1.20
A168(1)	0.37	0.29	± 0.062
A168(2)	0.80	0.52	± 0.086
A168(3)	0.11	0.062	± 0.016
A279	1.23	5.86	± 0.90
A671(1)	0.37	0.30	± 0.060
A671(2)	0.75	0.72	± 0.063
A671(3)	0.18	0.13	± 0.02
A690	1.42	3.61	± 0.84
A957	0.77	4.01	± 0.80
A971	1.12	7.33	± 1.50
A1177	1.09	1.35	± 0.32
A1213	1.64	4.93	± 0.64
A1291(1)	0.20	0.12	± 0.028
A1291(2)	0.33	0.21	± 0.06
A1291(3)	0.79	0.58	± 0.019
A1468	1.43	3.58	± 0.62
A1516	1.65	7.84	± 1.50
A1569	1.40	3.03	± 0.40
A1650	1.87	8.86	± 1.60
A1656	1.33	8.74	± 0.58
A1691	1.50	8.40	± 1.34
A1795	1.58	10.46	± 1.80
A1800	1.52	7.46	± 1.40
A1913	1.50	5.80	± 0.77
A1983	1.28	3.89	± 0.49
A1991	1.41	5.16	± 0.79
A2029	1.61	13.90	± 2.10
A2079	1.56	5.89	± 1.2
A2089	1.61	5.09	± 0.87
A2107	1.28	5.31	± 0.70
A2124	1.38	8.30	± 1.30
A2147	1.36	7.19	± 0.73
A2199	1.50	7.25	± 0.72
A2244	1.50	8.65	± 1.40
A2356	1.37	3.90	± 0.86
A2399	1.54	5.95	± 0.77
A2428	1.62	4.89	± 1.10
A2593	1.34	5.73	± 0.90
A2670	1.75	11.35	± 1.70

3.2 Luminosity Function analysis

As we already established, the luminosity function, $\Phi(L)$, of a cluster is the number density of galaxies per luminosity interval. Here we will directly estimate $\Phi(L)$ for each cluster of our sample and to this end we use the SDSS galaxy data which provide the apparent magnitudes, in 5 bands, of each galaxy, although in the current work we focuses only in the r-band magnitudes. We transform apparent magnitudes to absolute magnitudes using the well-known distance modulus, according to:

$$m_r - M = 5 \log_{10}(d_L) + 25 + K_r(z) + A_r \quad (3.3)$$

where m_r is the r-band apparent magnitude, M is the absolute magnitude, d_L is the distance modulus, $K_r(z)$ is the K-correction for the r-band, which is a function of redshift, and A_r is the Galactic absorption in the r-band. The K_r correction term is needed to convert the apparent magnitude of a galaxy to that in the rest-frame of the object, since the light that we detect from a source at a particular filter (r-band here) is emitted from different parts of the spectrum at the different redshifts. The only simplification we make in its use is that we assume that all cluster galaxies are ellipticals. For this process we use the Poginatti's (1997) tabulation of K-corrections, listed by redshift in bins of variable width. Therefore, we often use a linear interpolation between given values.

Galactic dust, that intervenes between the observer and the cluster, absorbs and scatters light, increasing the apparent magnitude of the galaxies. The term A_r corrects for this effect and depends mostly on the galactic latitude of the cluster.

Having transformed apparent magnitudes into absolute magnitudes, we plot for each cluster the appropriate distribution of M and we use a χ^2 minimization procedure to fit a Schechter luminosity function to each such cluster distribution. To this end we assume $\alpha=-1.25$ (Popesso et al. 2005) and we leave as a free parameters M_* . Once we estimate M_* , we transform it into luminosity by:

$$M_{\odot} - M_* = 2.5 \log_{10}(L_*/L_{\odot}) \quad (3.4)$$

using

$$M_* = -2.5 \log_{10} L_* + c \quad M_{\odot} = -2.5 \log_{10} L_{\odot} + c \quad (3.5)$$

The absolute magnitude of the Sun in the r-band is 4.67 and thus we finally obtain:

$$L_* = 10^{0.4(4.67 - M_*)} \quad (3.6)$$

We now describe how we estimate the normalization parameter ϕ_* . We use (a) the fact that the integral of the cluster $\Phi(L)$ can be considered as being equal to the total number density of observable galaxies contained in the cluster, and (b) that the observable galaxies are those contained within the specific limits of luminosity, L_{\min} , allowed by the magnitude limit of the SDSS catalogue. For each cluster the value of L_{\min} is the luminosity corresponding to the limiting apparent magnitude of the SDSS spectroscopic catalogue ($m_r \simeq 17.7$) at its redshift. To sum up, the formula used to estimate the number of observable galaxies in each one of our clusters is :

$$N_{\text{obs}} = V_{\text{clus}} \int_{L_{\min}/L_*}^{\infty} \Phi(L) dL = V_{\text{clus}} \phi_* \Gamma'(\alpha + 1, L_{\min}/L_*) \quad (3.7)$$

where V_{clus} is the volume covered by the cluster (which will be factored out in any case) and $\Gamma'(\alpha + 1, L_{\min}/L_*)$ is an incomplete Γ function. Therefore counting the cluster member galaxies, N_{obs} , with $L \geq L_{\min}$ we can estimate the normalization parameter by:

$$\phi_* = \frac{N_{\text{obs}}}{\Gamma(\alpha + 1, L_{\min}/L_*) V_{\text{clus}}} \quad (3.8)$$

Finally, the cluster total luminosity density is estimated by:

$$L_{\text{cluster}} = V_{\text{clus}} \int_0^{\infty} L \Phi(L) dL = V_{\text{clus}} \phi_* L_* \Gamma(\alpha + 2) = N_{\text{obs}} L_* \frac{\Gamma(\alpha + 2)}{\Gamma'(\alpha + 1, L_{\min}/L_*)} \quad (3.9)$$

In Table 3.2 we present the best-fit galaxy luminosity function parameters, the reduced χ^2 of the fit and the cluster total luminosity, provided by eq.(3.9).

The Luminosity function analysis is the most laborious part of this thesis. The diagrams, consist of a histogram of the absolute magnitude distribution of the cluster member galaxies and an analytical fit to the data of a Schechter-type function Here we present some of these diagrams, while the rest can be found in the Appendix C.

3.3 Correlations between Mass and Richness

In general one expects to have more galaxies in more massive clusters. Therefore one expects to have a strong correlation between the dynamical mass of clusters and their richness, measured either by the number of bright galaxies, or by Abell richness class.

To this end we plot in Fig.(3.2) the scatter diagrams between the cluster dynamical mass (x-axis) and N_g or R_A (y-axis) and we apply the usual Spearman and Pearson correlation analysis to quantify if such correlations do exist among the above cluster parameters.

Indeed, there seems to be an increase in a cluster's mass when either the number of galaxies it contains or the Abell richness class is larger. That is to say, rich clusters are more massive than the poorer ones.

To estimate the Pearson coefficient we use the following formula:

$$R_p = \frac{\sum(x_i - \bar{x})(y_i - \bar{y})}{\sqrt{\sum(x_i - \bar{x})^2} \sqrt{\sum(y_i - \bar{y})^2}} \quad (3.10)$$

where x_i are the values plotted on the x-axis, and y_i the values of the masses (or richness classes) plotted on the y-axis. Obviously, \bar{x} and \bar{y} are the mean values of those variables.

TABLE 3.2: Best-fit Schechter luminosity function parameters and χ^2/dof values.

Name	M_*	ϕ_*	$L_*(10^{10} h_{72}^{-2} L_\odot)$	χ^2/df
A85	-21.62	49.30	3.28	0.80
A279	-21.45	41.77	2.80	1.23
A690	-21.18	50.91	2.18	0.93
A957	-21.20	25.60	2.22	0.72
A971	-21.44	40.05	2.77	0.51
A1177	-21.60	13.25	3.22	1.30
A1213	-21.63	44.16	2.85	0.91
A1468	-21.10	37.33	2.03	0.89
A1516	-21.39	41.94	2.65	0.55
A1650	-21.44	43.57	2.77	0.75
A1656	-22.15	57.82	6.48	0.80
A1691	-21.63	38.32	3.31	0.89
A1795	-21.60	44.93	3.22	0.50
A1800	-21.79	34.09	3.83	1.26
A1913	-21.62	39.38	3.28	0.50
A1983	-21.60	43.61	3.22	0.70
A1991	-21.64	40.95	3.34	1.20
A2029	-21.67	50.27	3.43	0.80
A2079	-21.42	35.20	2.72	0.66
A2089	-21.48	34.70	2.88	0.72
A2107	-21.44	35.85	2.77	0.65
A2124	-21.34	37.95	2.53	0.60
A2147	-22.02	44.38	4.74	1.25
A2199	-21.67	41.93	3.43	1.75
A2244	-21.78	45.81	3.80	0.81
A2356	-21.54	39.31	3.04	0.95
A2399	-21.60	40.35	3.22	0.70
A2428	-21.15	65.59	2.12	0.50
A2593	-21.44	33.17	2.78	1.65
A2670	-21.75	54.58	3.69	0.90

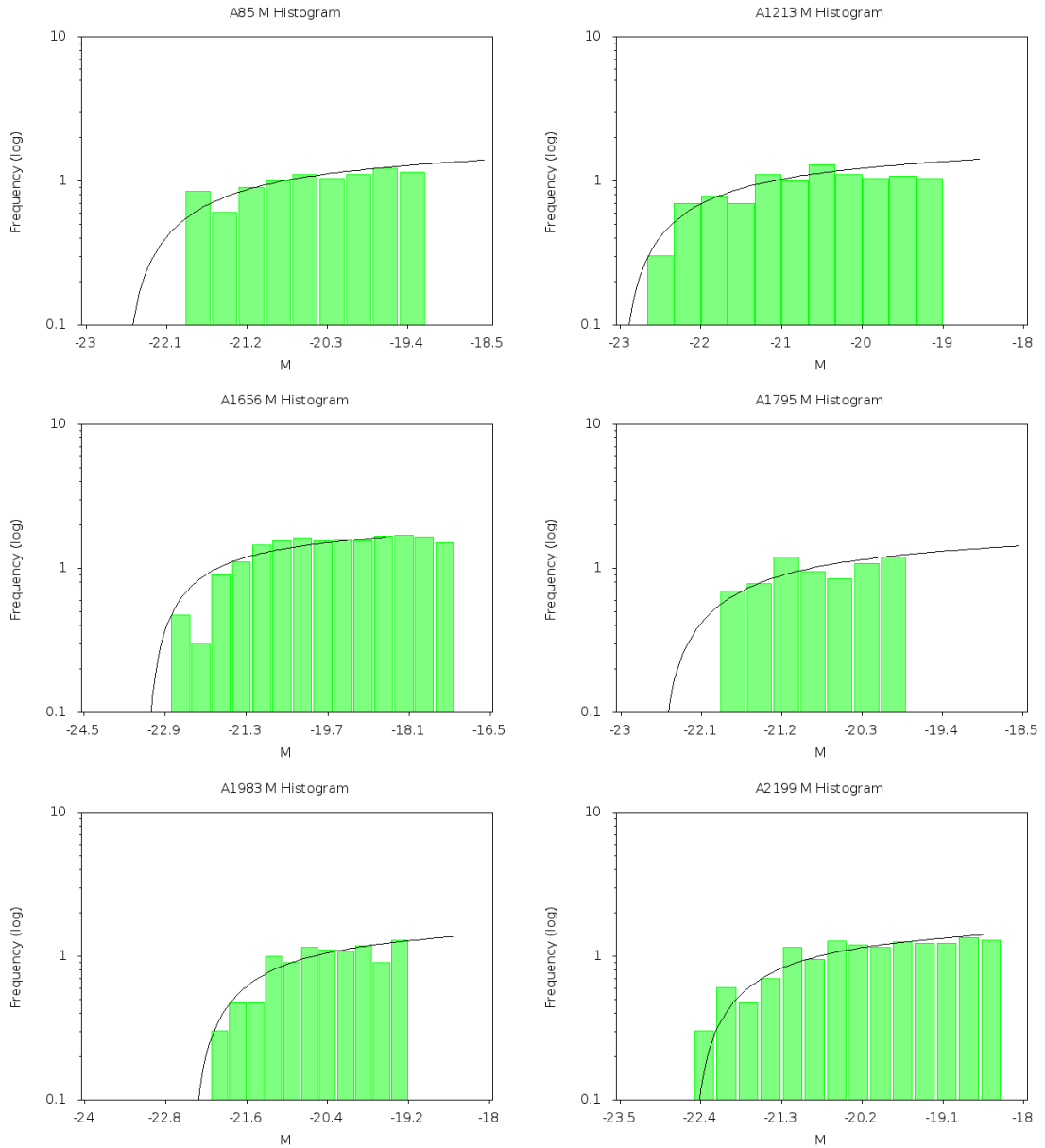


FIGURE 3.1: From top left to bottom right: Galaxy luminosity functions of the clusters A85, A1213, A1656, A1795, A1983 and A2199.

Similarly, in order to estimate the Spearman correlation coefficient, we use:

$$r_s = 1 - \frac{6 \sum D^2}{N^3 - N} \quad (3.11)$$

where D is the difference between ranks ($x_i - y_i$). Note that the Pearson (or Spearman) coefficient, take values between -1 and 1. A value equal to 1 means that we have a totally positive correlation between the two parameters, -1 means that we have a totally negative correlation, whilst 0 means that we have no correlation at all.

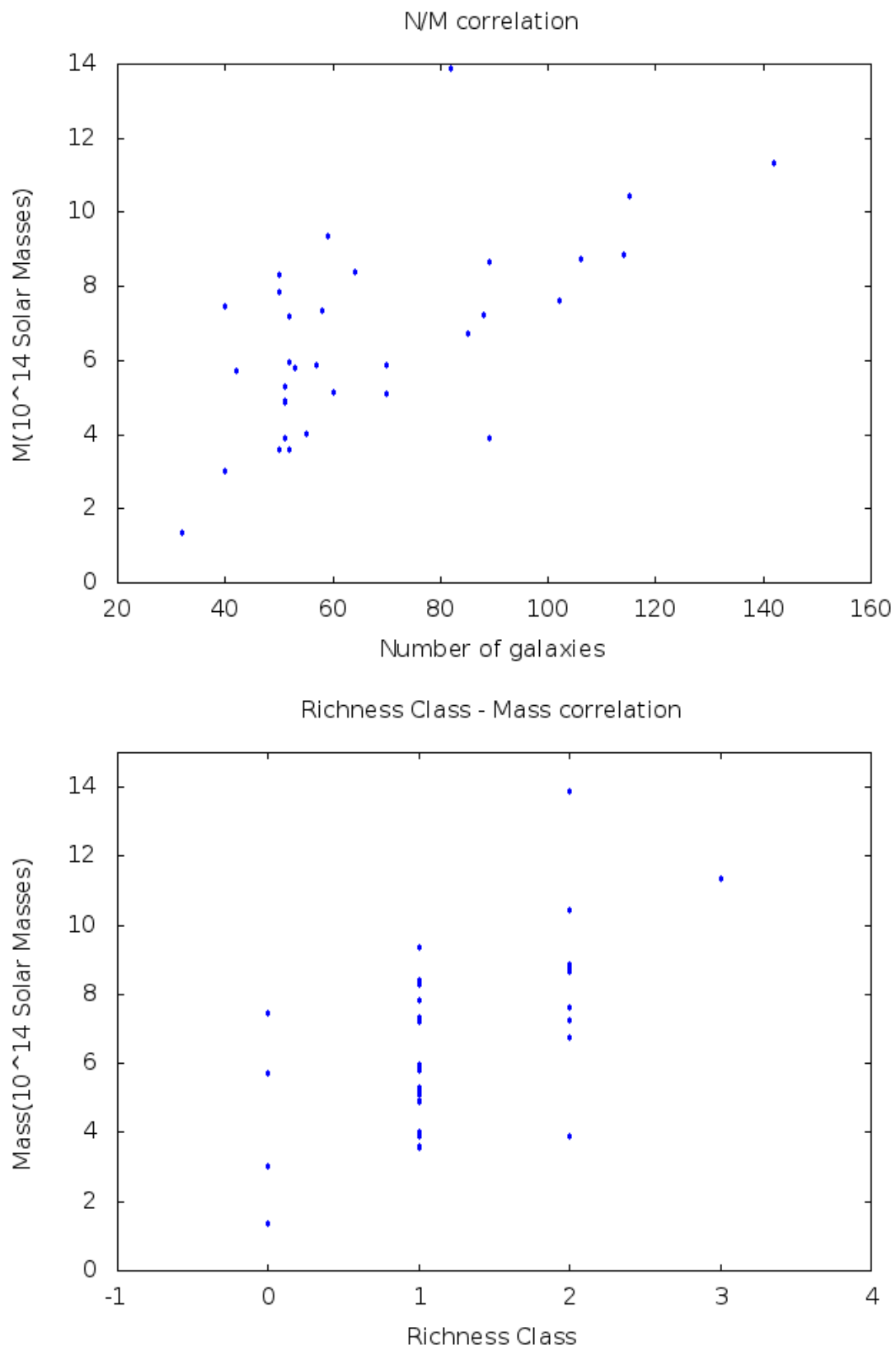


FIGURE 3.2: Left Panel: Dynamical mass versus number of bright cluster member galaxies. Right Panel: Dynamical mass versus Abell richness classes, for the clusters of our sample.

The specific values of the Pearson and Spearman coefficients for the two diagrams and their probability (P) of being such due to chance are shown in Table 3.3).

TABLE 3.3: Correlation coefficients for N-M and N-R.

Diagram	R_p	P_p	R_s	P_s
N_g -Mass	0.622	0.00011	0.577	0.00043
R_A -Mass	0.605	0.00019	0.564	0.00063

It is easy to notice that there is a quite strong correlation between the cluster parameters tested, as well as a very high probability that these correlations are real and not due to chance. We therefore claim that not only is there a relation between N_g or R_A and the dynamical cluster Mass but there is also quite a certainty that these relation reflect real physical processes.

3.4 Cluster M/L Ratios & Ω_m

We calculate the cluster M/L ratios by simply dividing the virial masses (Table 3.1) with the L_{cluster} derived in section 3.3. The cluster M/L are listed in Table ??).

3.5 Cluster M/L Ratio Analysis

First, we demonstrate in this section the table of M/L ratios that we have. We calculate the cluster M/L ratios simply by dividing the virial cluster masses (see chapter 2) with the L_{cluster} (Table ??) we found before. The M/L Table has as follows :

We also plot the derived M/L ratios as a function of cluster mass in Fig. (3.3). We also show the uncertainty of each M/L value, derived by propagation of errors. What is expect is to have a roughly linear dependance up to some characteristic cluster mass, above which a "plateau" should appear (see Bachall 1999). This is due to a well know effect, where the M/L ratios is an increasing function of cosmic structure mass (starting from galaxies, groups of galaxies and clusters of galaxies; see also Fang & Xu 1999), up to a mass over which the cosmic structure has the global (universal) value of M/L , which then can be used to place cosmological constraints, as we will see further below. Indeed we see such an increasing trend of M/L with M .

In order now to estimate the value of the Ω_m parameter, which is the final goal of this thesis, we must assume, as already discussed, that the M/L ratio of the clusters we

TABLE 3.4: Cluster M/L Ratios and uncertainties.

Name	M/L(hM_\odot/L_\odot)	M/L uncertainties(hM_\odot/L_\odot)
A85	471.15	± 34.2
A279	408.08	± 32.9
A690	264.45	± 25.6
A957	573.52	± 52.3
A971	537.29	± 51.5
A1177	258.08	± 27.4
A1213	318.80	± 29.5
A1468	385.09	± 31.0
A1516	574.53	± 49.9
1650	596.89	± 58.8
A1656	230.46	± 21.2
A1691	540.22	± 56.3
A1738	554.96	± 55.5
A1795	589.75	± 56.9
A1800	465.27	± 42.4
A1913	366.25	± 33.7
A1983	225.97	± 21.1
A1991	307.62	± 28.9
A2029	656.68	± 70.8
A2079	500.29	± 49.1
A2089	414.94	± 36.7
A2107	434.74	± 45.6
A2124	704.01	± 72.3
A2147	278.72	± 22.1
A2199	410.63	± 35.6
A2244	405.27	± 37.7
A2255	558.38	± 51.1
A2356	265.62	± 34.3
A2399	373.58	± 36.1
A2428	285.87	± 22.2
A2593	507.11	± 51.5
A2670	458.82	± 43.2

calculated correspond on average to the global M/L_{univ} ratio of the Universe, which is given by:

$$\left(\frac{M}{L}\right)_{\text{clus}} = \left(\frac{M}{L}\right)_{\text{univ}} \implies \left(\frac{M}{L}\right)_{\text{clus}} = \frac{\rho_0}{\langle \mathcal{L} \rangle} = \frac{\Omega_m \rho_{\text{tot}}}{\langle \mathcal{L} \rangle} \quad (3.12)$$

where ρ_0 is the mean mass density of the Universe, ρ_{tot} is the mean total mass-energy density of the Universe (to which all sources of gravity contribute), and $\langle \mathcal{L} \rangle$ is the mean luminosity density of the Universe. The value of ρ_{tot} is given by the first Friedmann's equation and it is:

$$\rho_{\text{tot}} = \frac{3H_0^2}{8\pi G} = 2.775 \times 10^{11} M_\odot h^2 \text{Mpc}^{-3} \quad (3.13)$$

where $H_0 = 100h \text{ km s}^{-1} \text{ Mpc}^{-3}$.

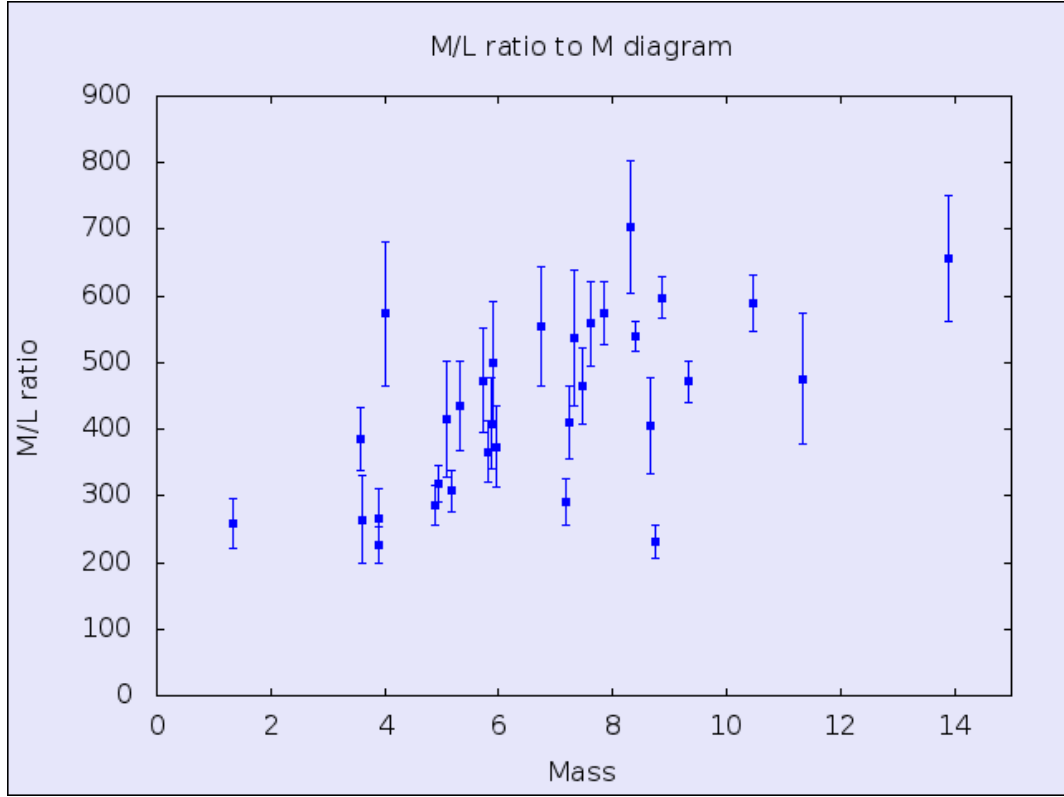


FIGURE 3.3: Mass to M/L diagram.

In order to derive the mean luminosity density of the Universe, $\langle \mathcal{L} \rangle$, we use the field luminosity function of Montero-Dorta et al. (2008) and its best-fit Schechter parameters: $\phi_* = 0.009h^3 = 0.00336$ and $M_* = -20.73 + 5 \log_{10} h$. We first calculate, via eq.(3.6), the value of L_* : $L_* = 1.4454 \times 10^{10} h^{-2} L_\odot$, and then we integrate the 1st moment of the field luminosity function to obtain the mean luminosity density

$$\langle \mathcal{L} \rangle = \phi_* L_* \Gamma(a + 2) = \phi_* L_* \Gamma(0.77) = 1.5607 \times 10^8 h L_\odot \text{Mpc}^{-3} \quad (3.14)$$

reminding that the normalization is given by $H_0 = 100h \text{ km s}^{-1} \text{ Mpc}^{-1}$. As already mentioned, the M/L ratio that enters in eq.(3.12) corresponds to the average ratio of the Universe, which we take it to be that of clusters of galaxies. Thus, we will use two different values for the cluster M/L : the mean M/L ratio over all clusters in our sample and the value corresponding to the rough “plateau” seen in Fig.(3.3), ie.,

$$\left(\frac{M}{L} \right)_{\text{clus,mean}} \approx 423 \pm 37.8(1 - \Delta) h_{72} \frac{M_\odot}{L_\odot} \pm 37.8 \quad (3.15)$$

and

$$\left(\frac{M}{L} \right)_{\text{clus,plateau}} \approx 600 \pm 54.1(1 - \Delta) h_{72} \frac{M_\odot}{L_\odot} \quad (3.16)$$

where Δ is the correction factor introduced in eq.(3.2) which we take $\Delta \simeq 0.19$ (Girardi

et al. 1998), while here we have also used the nominal value of the Hubble constant: $H_0 = 72h_{72} \text{ km s}^{-1} \text{ Mpc}^{-1}$.

Finally, using eq.(3.12) and solving for Ω_m we have:

$$\Omega_m = \frac{\langle \mathcal{L} \rangle}{\rho_{\text{tot}}} \left(\frac{M}{L} \right)_{\text{clus}} = 0.00078 \left(\frac{M}{L} \right)_{\text{clus}} \quad (3.17)$$

from which, after taking into account the different H_0 normalizations, we obtain:

$$\Omega_m = 0.27 \pm 0.02 \quad \text{and} \quad \Omega_m = 0.38 \pm 0.04$$

respectively.

The first result is excellent consistency with the values derived for a large variety of cosmological probes. However, the second is somehow higher. We attribute this difference in the crude estimation of the cluster virial mass and total luminosity, since we have used a constant slope α of the Schechter luminosity function, but also on the lack of sufficient data for some of the clusters. There is certainly room for improvement on which we will indulge in the future.

Chapter 4

Conclusions

In this final chapter, we will review what we accomplished and focused in this thesis and we will offer some comments and remarks on the topics analysed throughout. By discussing our results, we will attempt to assess whether they are accurate enough and what are the limitations of the methods used. Finally, we will make some proposals concerning future research on the field and we will mention possible improvements and additions that we wish to indulge into in the future.

4.1 Overview of the thesis work

Starting with the first chapter, we presented a small introduction on clusters of galaxies. At first, we provided information on what a cluster is, what are its basic physical properties and why it is important as a structure in the Universe. We noted that clusters are the most massive virialized structures known and that they are even up to this day a major source of study when it comes to dark matter and the cosmological parameters in general. Secondly, we gave some insight on the way clusters form and evolve. The most important elements of a cluster's life and evolution were discussed, at least according to the most popular theories. Then, we also presented two different classifications of clusters, depending on their shape/appearance and their richness. Moreover, the first chapter contains a description of the main methods used to calculate a cluster's total mass. As noted, these methods are based on the virial theorem (based on optical spectroscopic observations), on the Euler equation (ie., using the X-ray emitting ICM gas as a tracer of the potential) and the gravitational lensing. We focused on the first method which is the method used in this thesis to calculate the total cluster masses. We also presented briefly the notion of the galaxy luminosity function, explaining that it represents the number density of galaxies in luminosity intervals.

The second chapter was dedicated to presenting the main sets of observational data used in this thesis and their processing. We consider a galaxy to be a candidate member of a cluster if it appears within an area (on the sky) of about $1.5 h_{72}^{-1}$ Mpc around the cluster's core and has a velocity within a ± 2000 km/s of the central cluster velocity. We derived the galaxy velocity dispersion of each cluster in our sample and presented for each the normalised velocity histograms, fitted with the best-fit Gaussian, which help us trim the galaxy distribution by excluding outliers that have velocities beyond the 3σ Gaussian limit. In general terms, the velocity dispersion values estimated, are comparable to dispersions measured in other scientific papers.

In the third chapter we used the Virial theorem to calculate the dynamical cluster masses and their virial radii. The masses obtained are in the region of $10^{14} h_{72}^{-1} M_{\odot}$ which is consistent with other studies. We proved that the dynamical cluster mass correlates strongly with the number of galaxies in the cluster (and also with another measure of its richness), as it should. We also presented the galaxy luminosity function analysis and estimated for each cluster the best-fit parameters of the Schechter luminosity function, i.e., the characteristic absolute magnitude M_* with the corresponding characteristic luminosity L_* as well as the normalization factor ϕ_* . To obtain the total luminosity of a cluster in solar luminosities, we go through a relatively complex procedure that provides values in the region of $10^{12} h_{72}^{-2} L_{\odot}$, consistent with that of other studies.

Finally, we estimated the mass to light ratio for each cluster, M/L , and compared it with the universal value to estimate the value of the cosmological density parameter, Ω_m , which was the aim of this thesis. The values found are in good agreement with those of other cosmological probes, although somewhat higher. In general though, we can conclude that the results obtained throughout this thesis, are satisfactory and the level of convergence to the those of other similar studies is quite impressive if one takes into account the necessary over-simplifications that we have used.

4.2 Future research

Although this thesis has achieved its initial goals, there is still room for improvement. In the near future, we intend to study the subject at hand even more intensively and to a higher detail by improving both the virial mass estimates and the luminosity function analysis. To this end,

- we will attempt to estimate the correction factor Δ for each cluster individually, in order to provide a better mass estimate, and

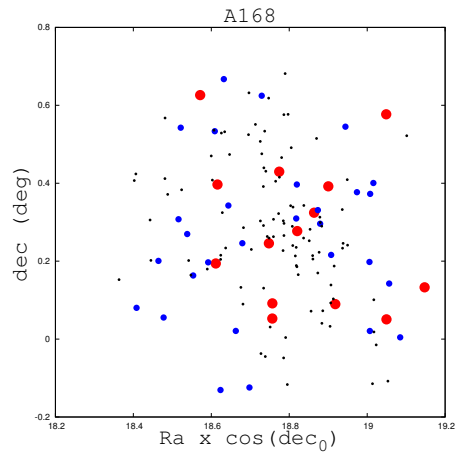
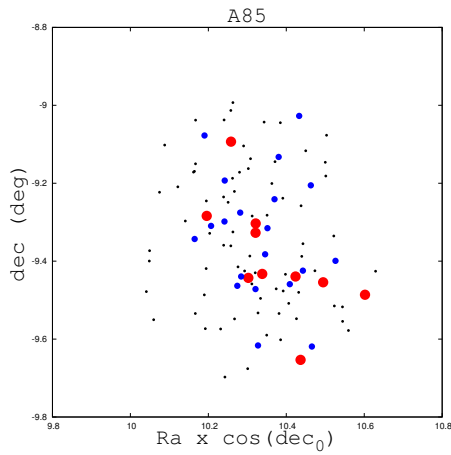
- we will iterate the whole luminosity function analysis, by allowing also the slope α as a free parameter to be fitted by the χ^2 minimization procedure and thus obtain more accurate values of the Schechter parameters and consequently of the $L_{cluster}$.

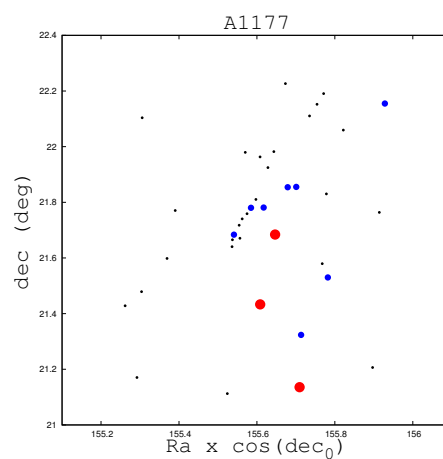
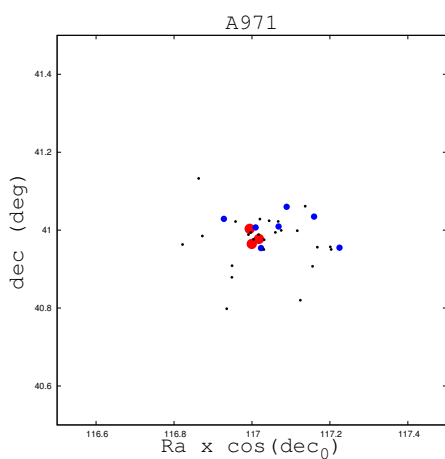
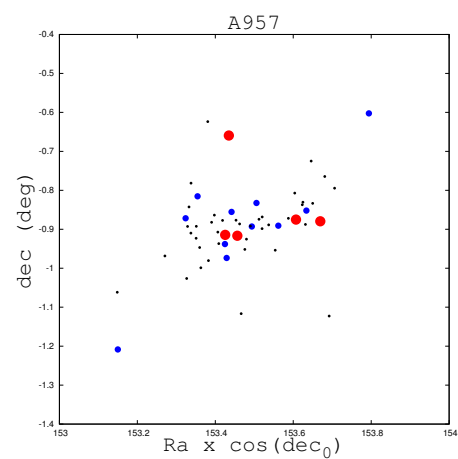
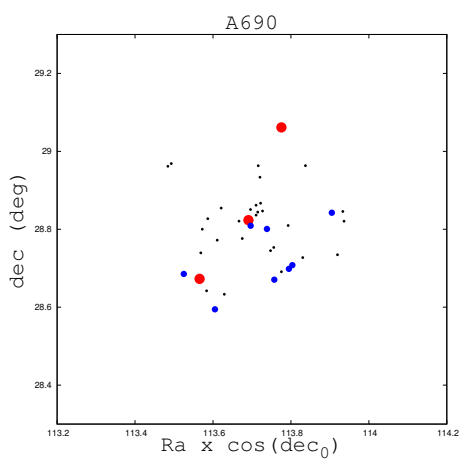
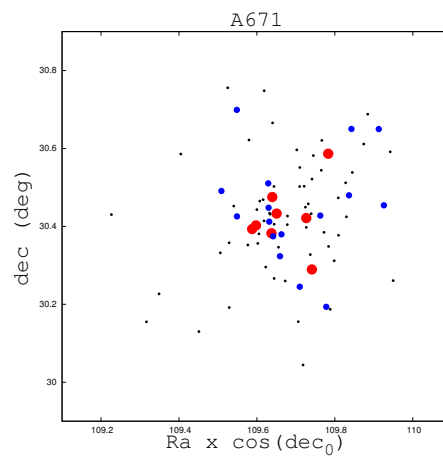
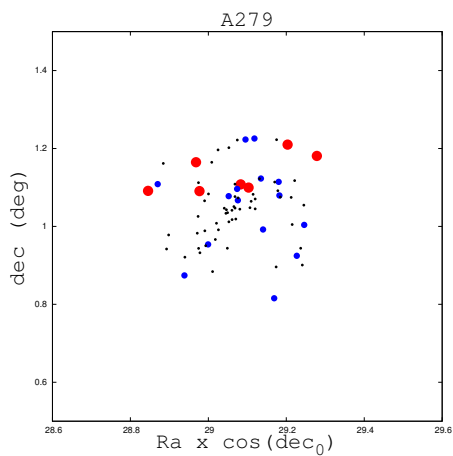
The above improvements will all affect the final value of Ωm and its uncertainty.

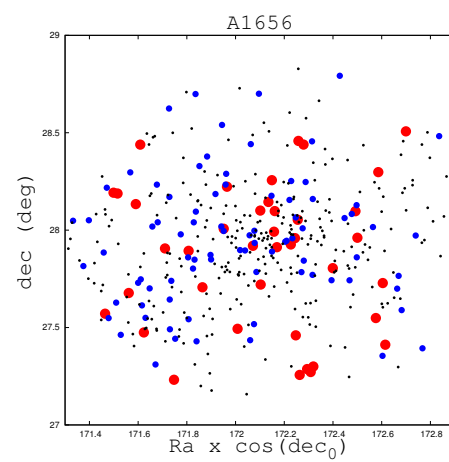
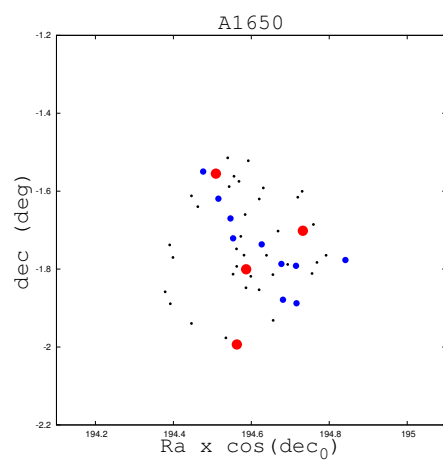
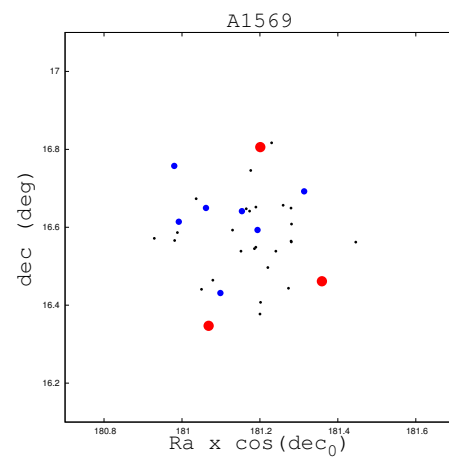
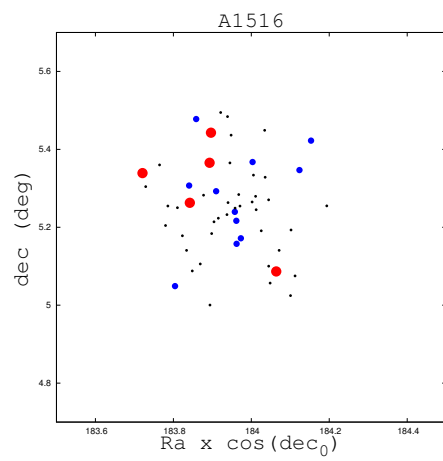
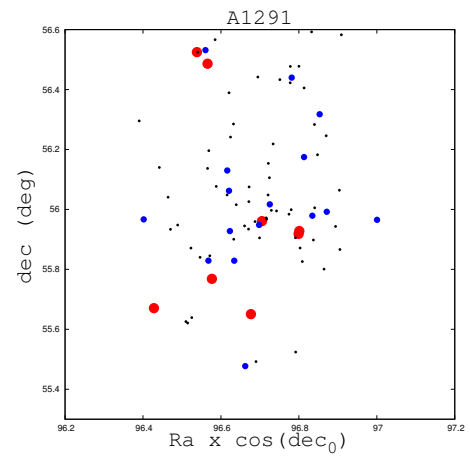
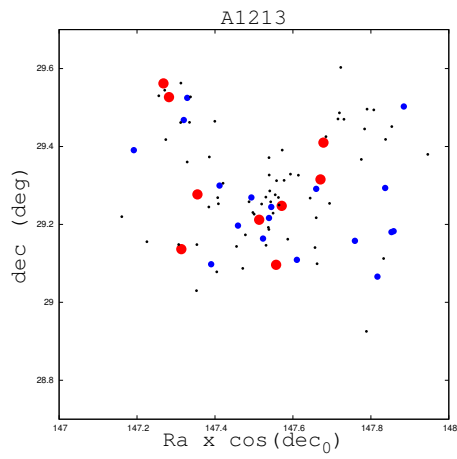
Appendix A

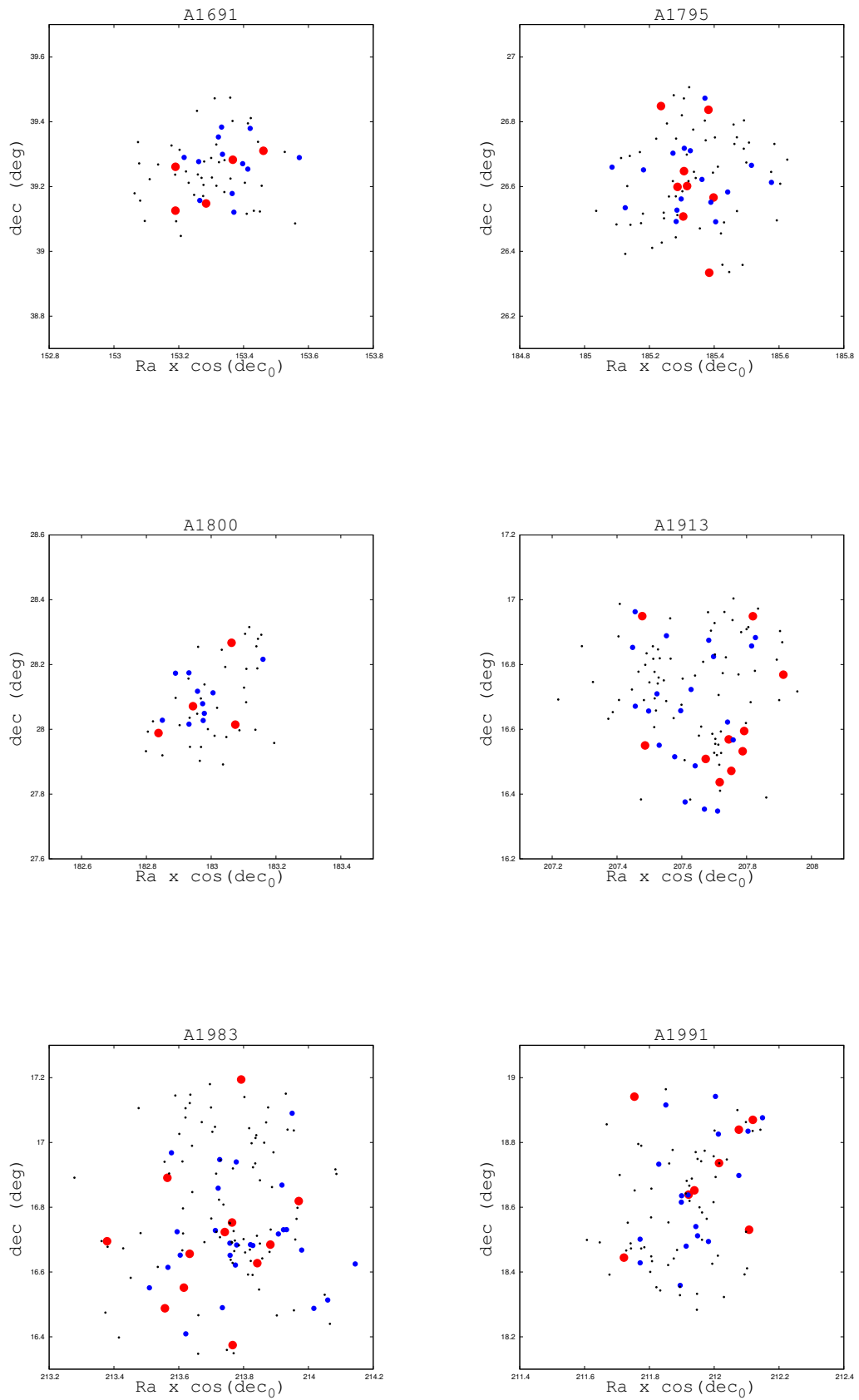
Equal Area Projection Diagrams

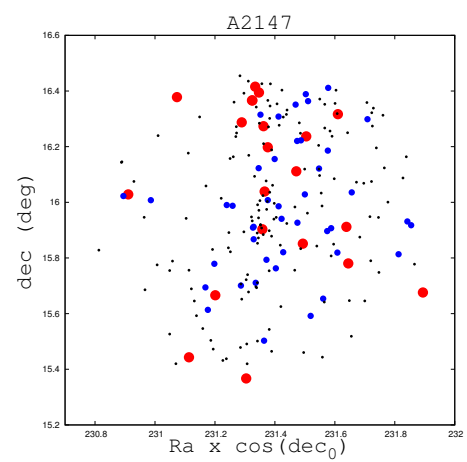
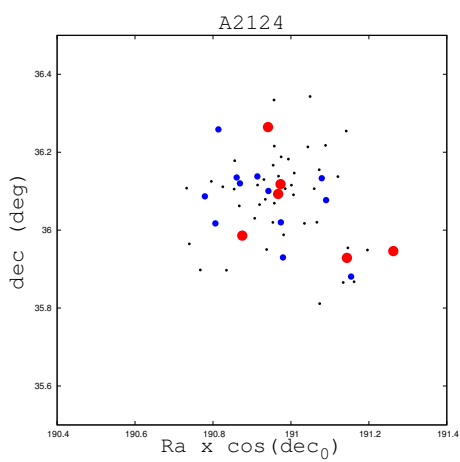
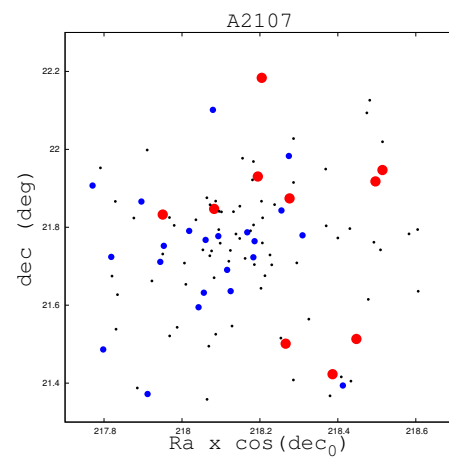
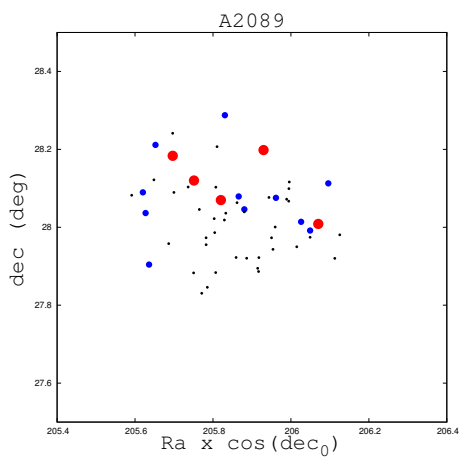
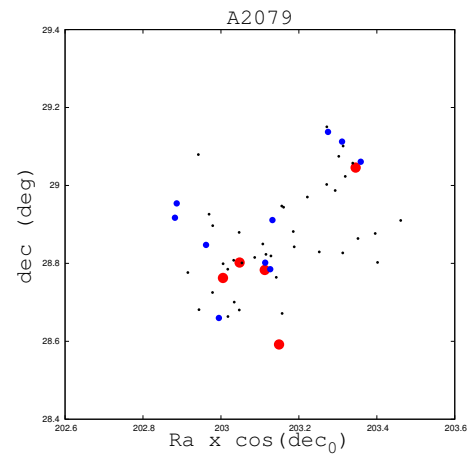
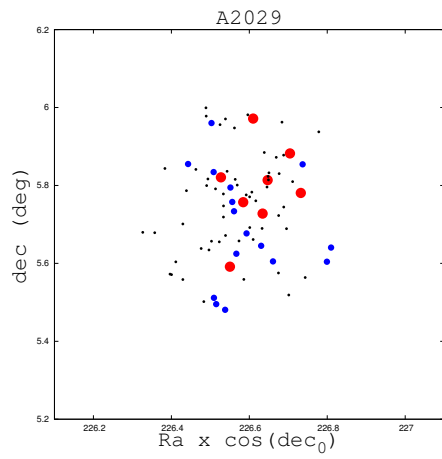
In this appendix, we present equal area projection diagrams of the galaxy distribution in each of our Abell clusters. The x-axis depicts the product of the right ascension with the cosine of the declination of the clusters center, while the y-axis corresponds to the declination coordinate.

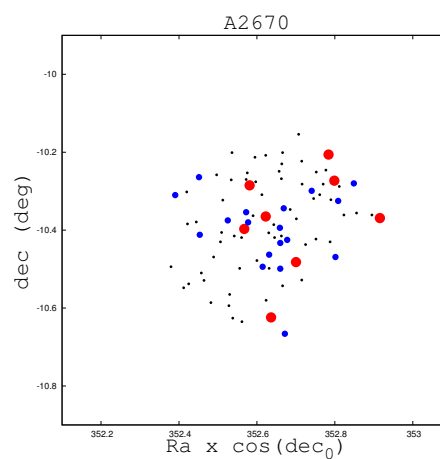
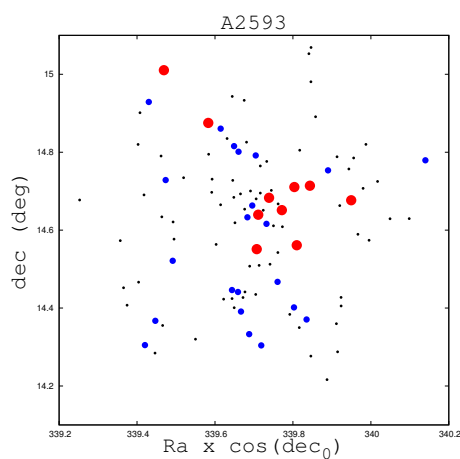
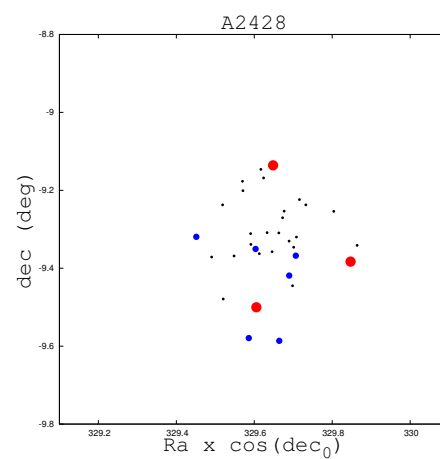
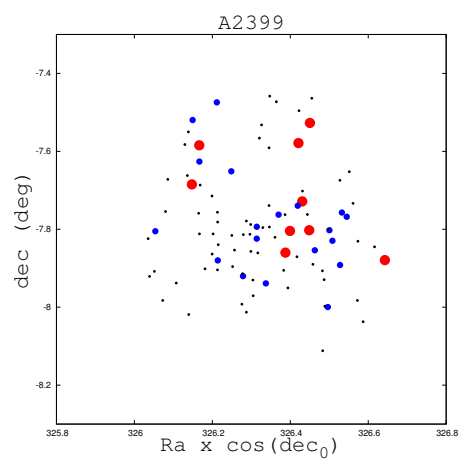
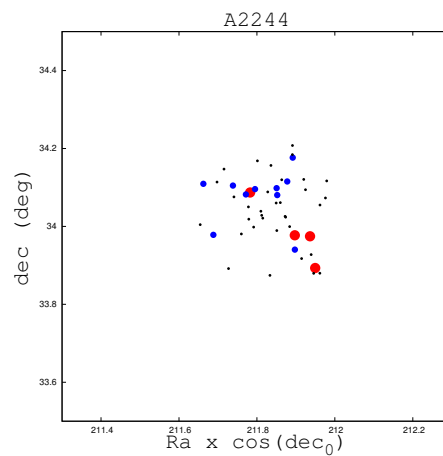
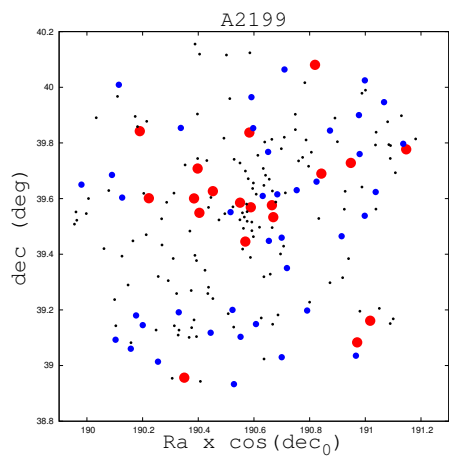


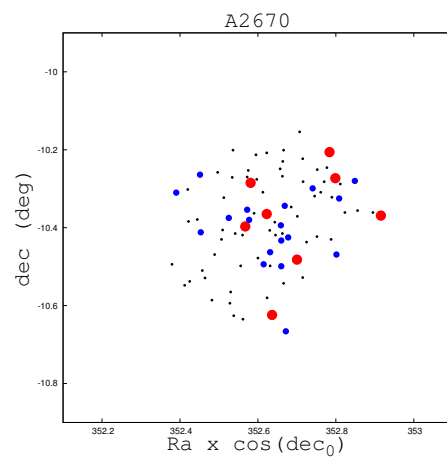
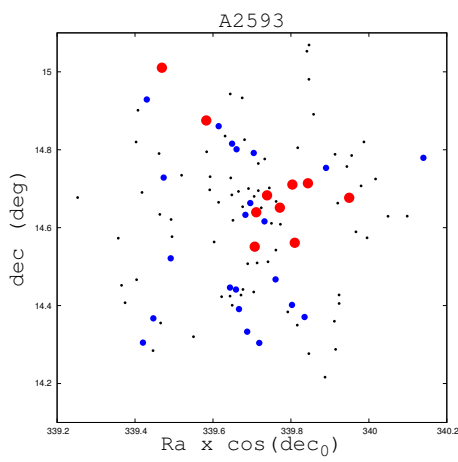
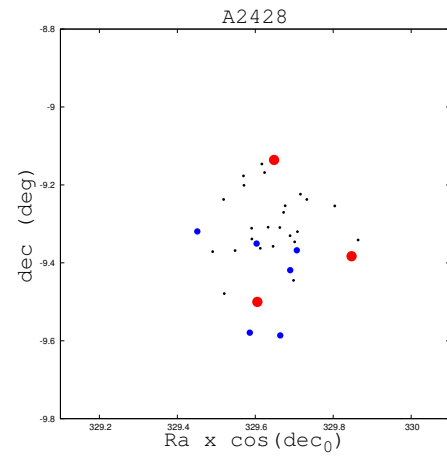
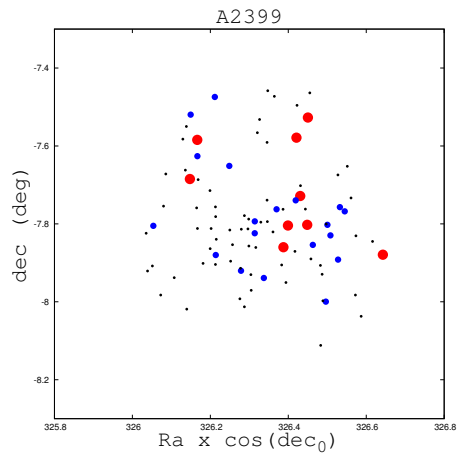








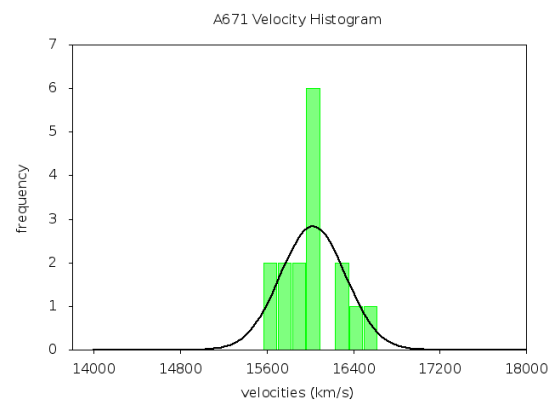
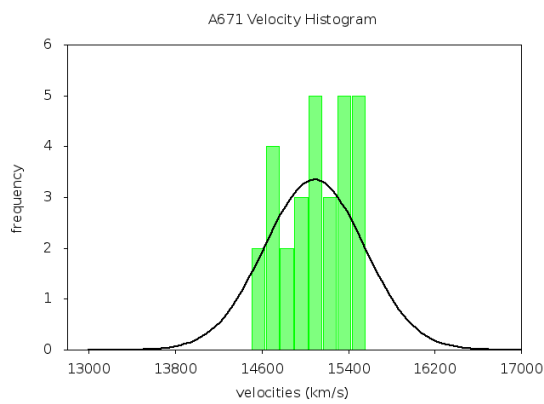
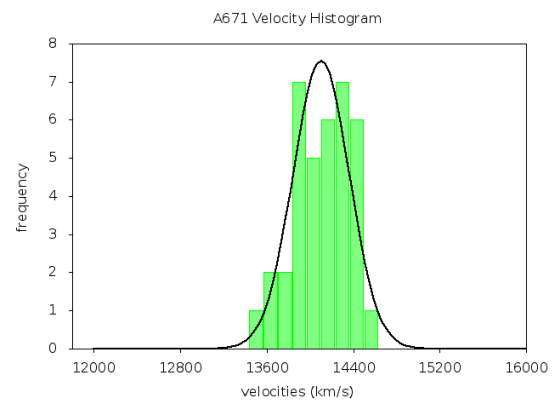
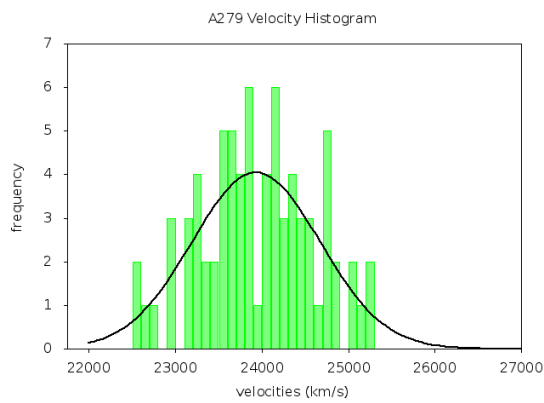
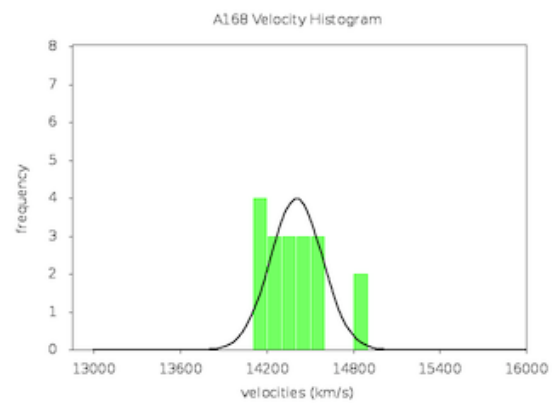
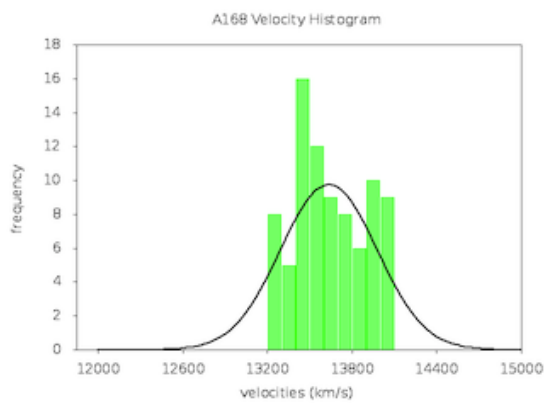
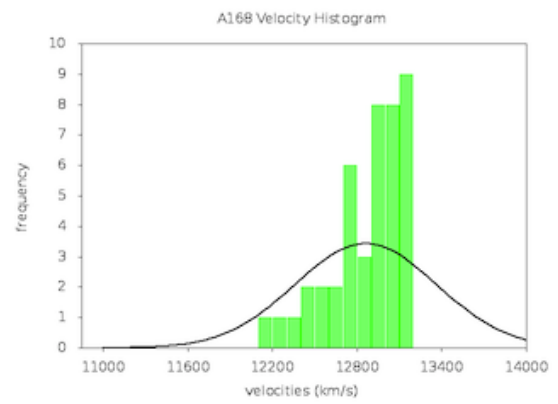
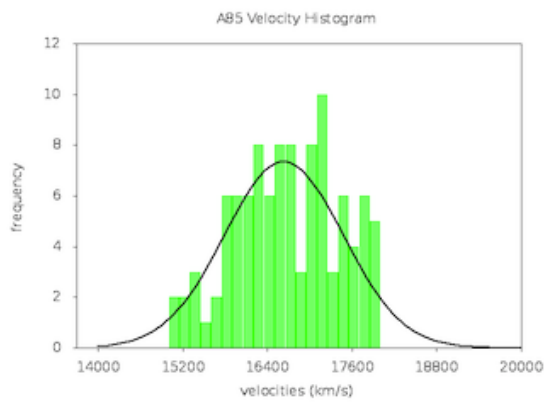


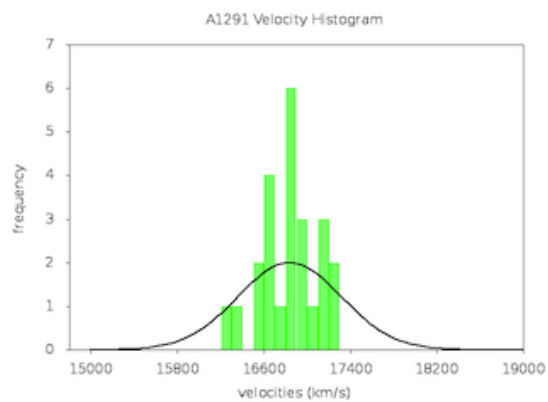
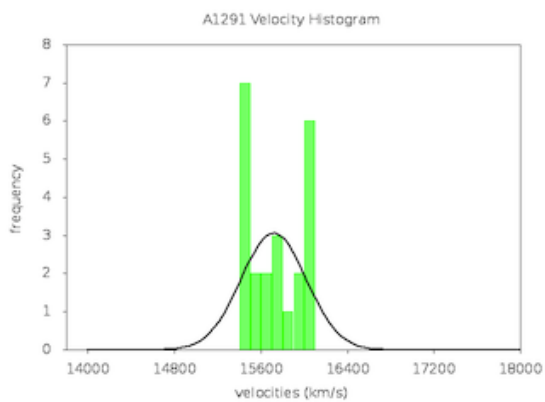
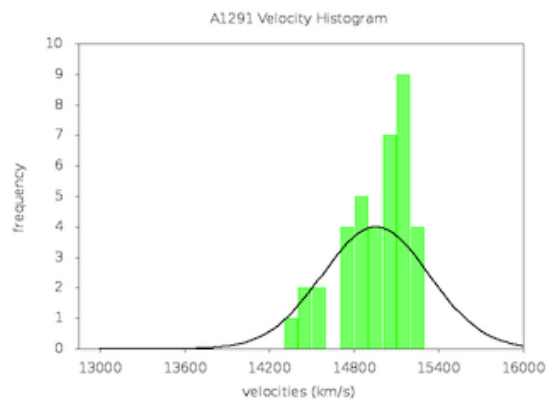
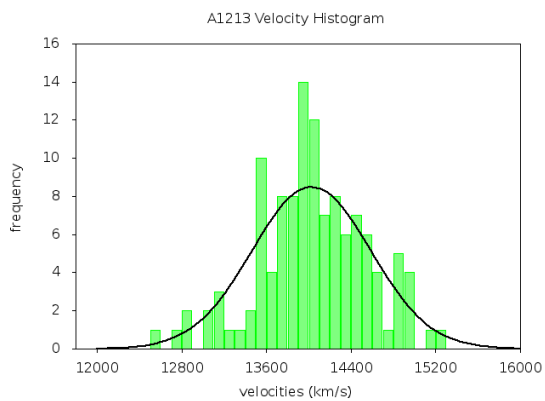
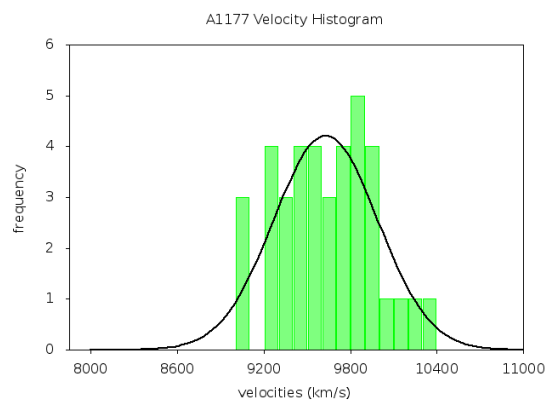
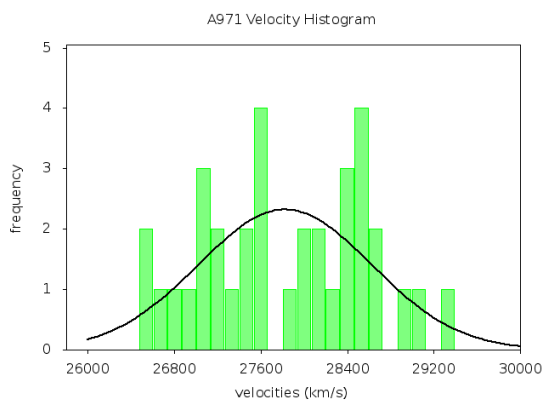
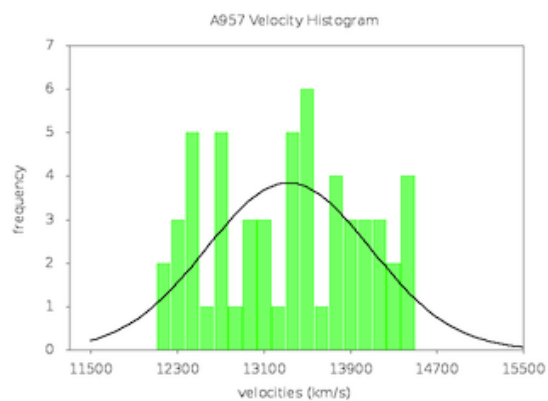
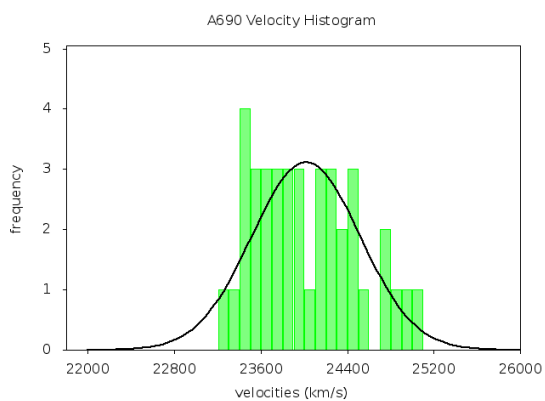


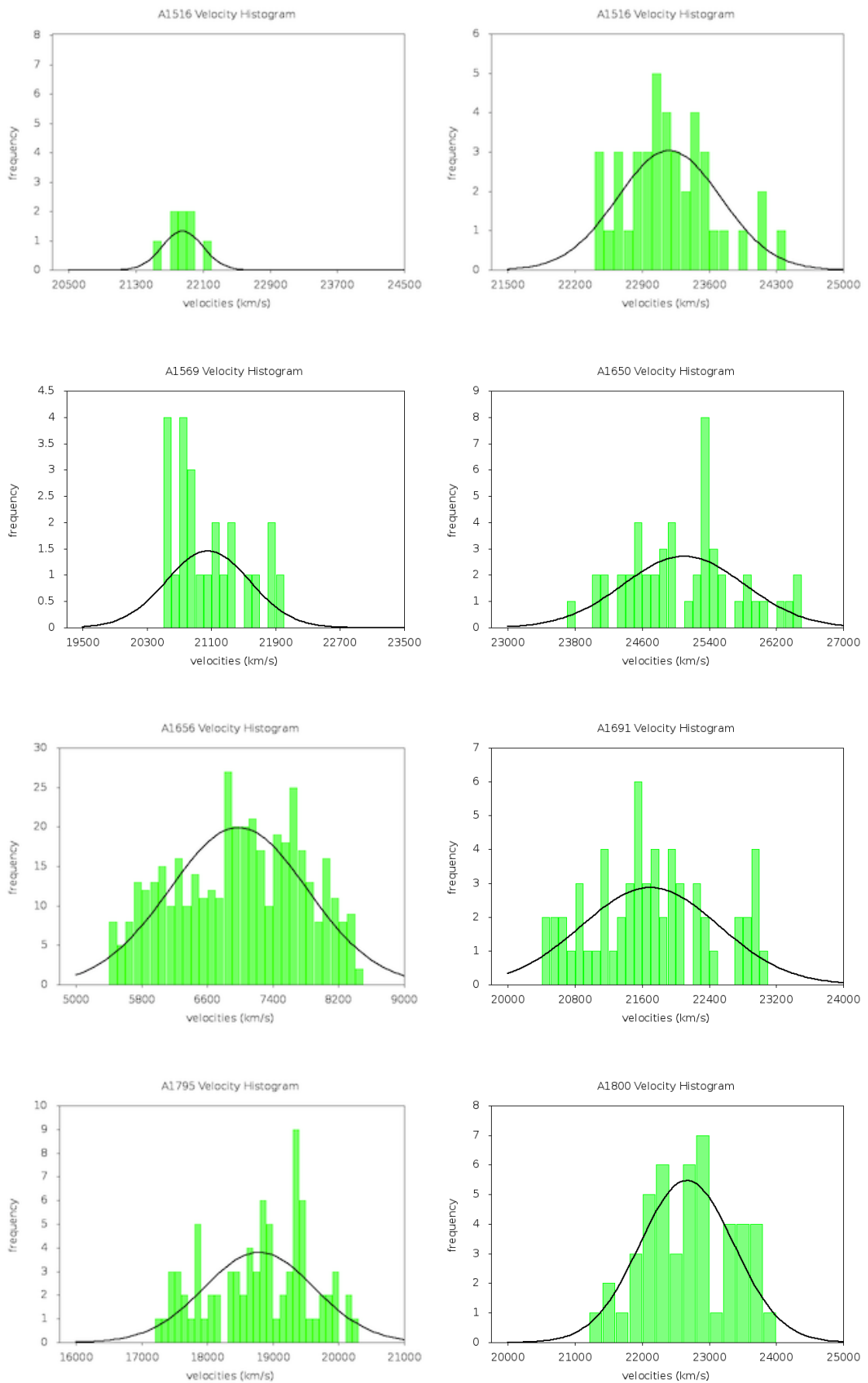
Appendix B

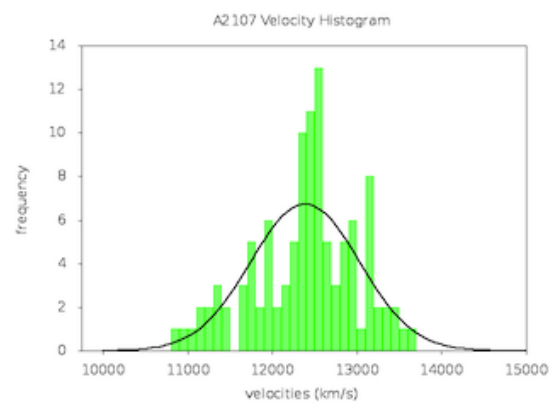
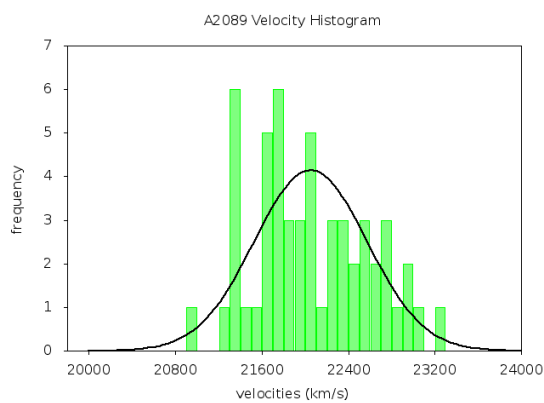
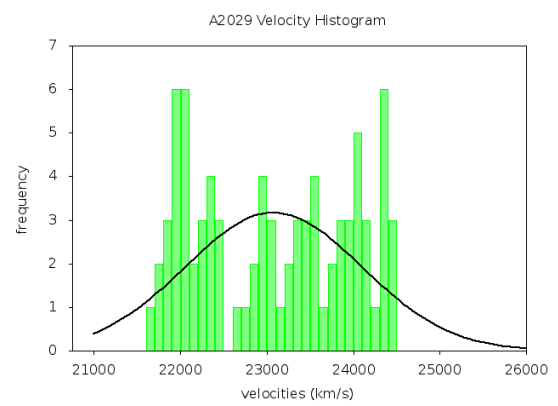
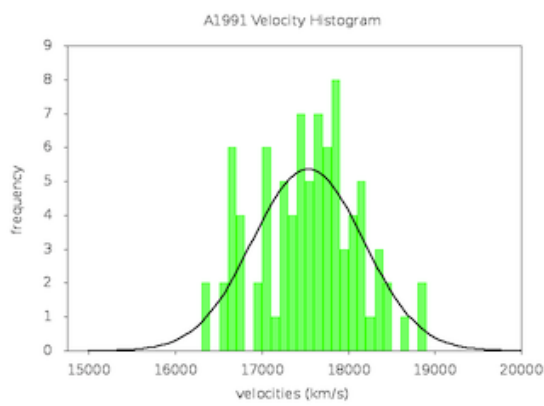
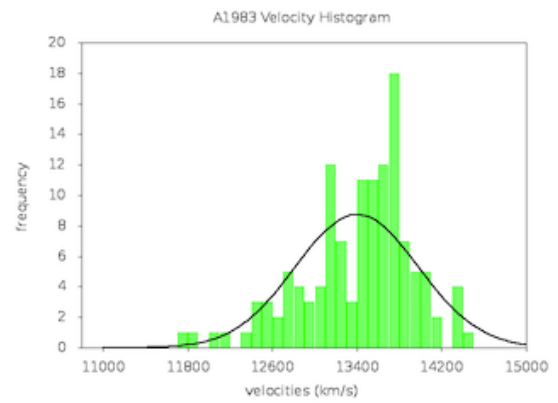
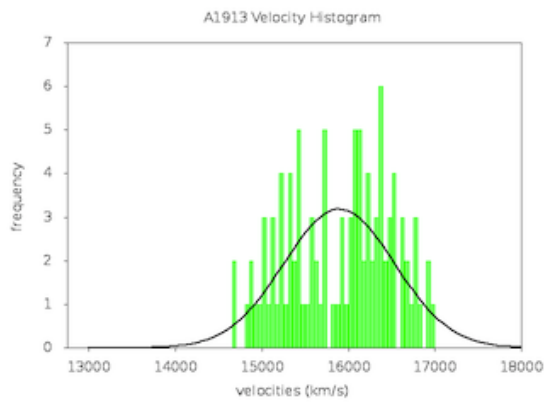
Velocity Dispersion Diagrams

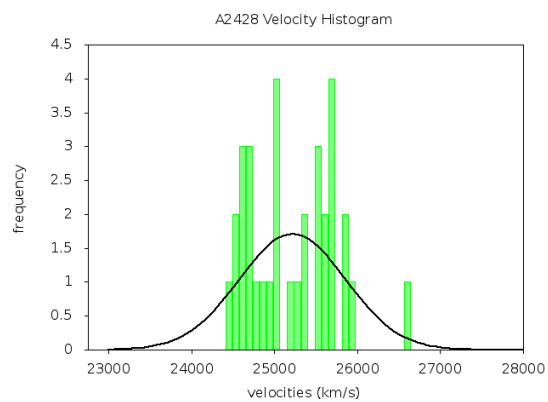
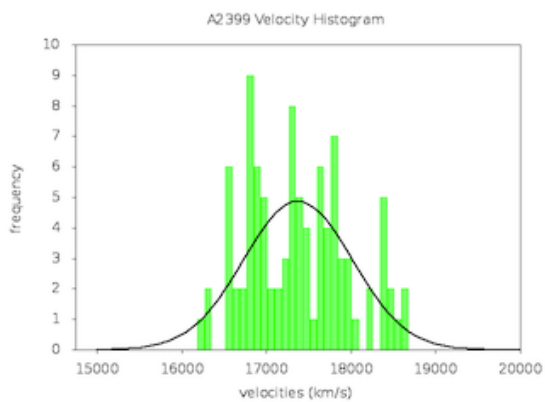
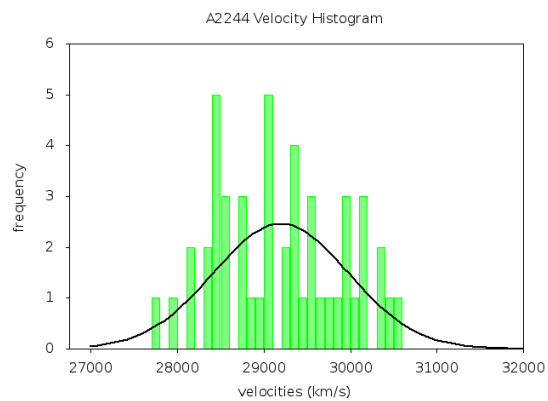
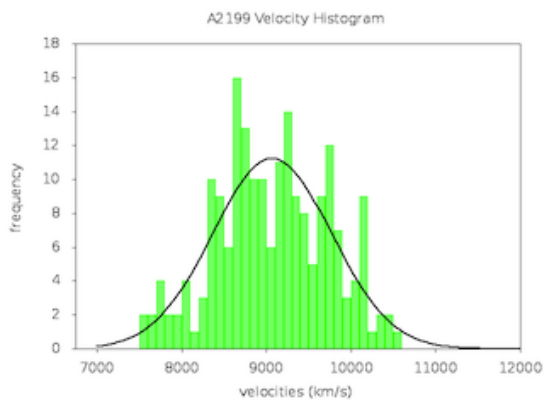
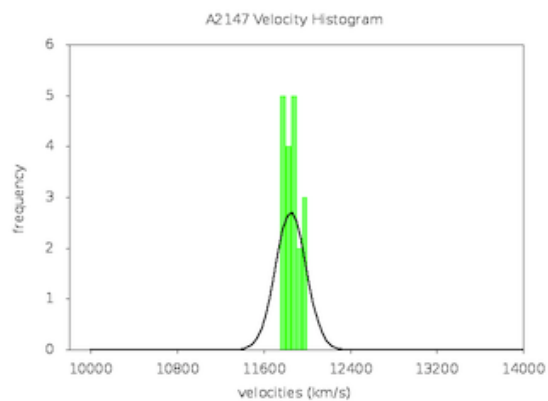
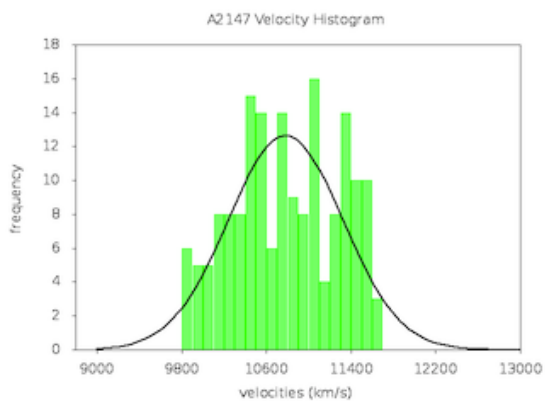
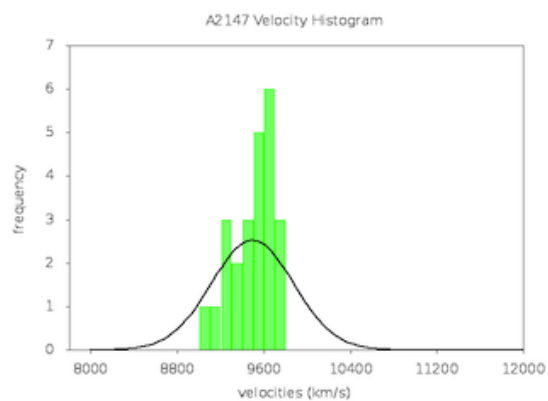
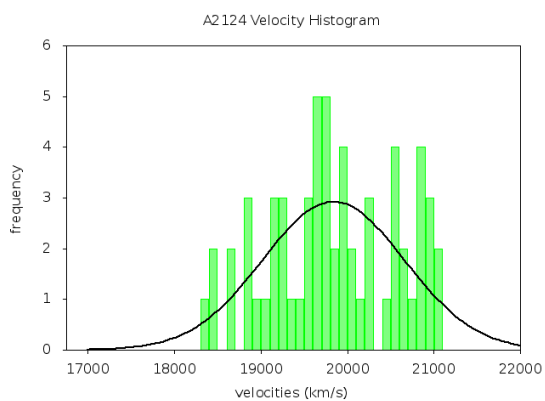
In this Appendix, we present the velocity dispersion diagrams for each of our Abell clusters. Note here that the central velocity (around which our histograms are plotted) is the mean velocity of each cluster. The x-axis depicts the galaxy velocity with respect to the cluster center and the y-axis depicts the frequency (number of galaxies corresponding to each velocity interval). It is important here to underline that some of our clusters are further divided into smaller groups of galaxies, each with its separate central (mean) velocity. Wherever this is the case, it is described in the caption that follows the diagram.

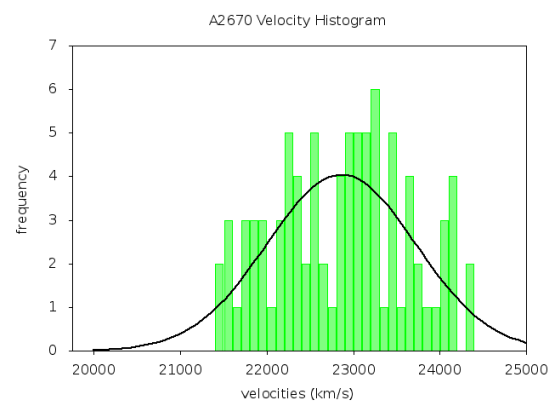
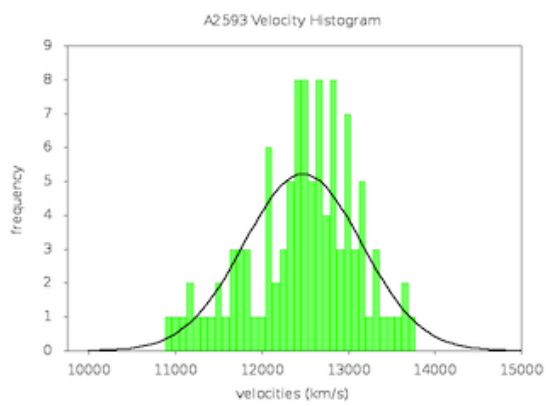








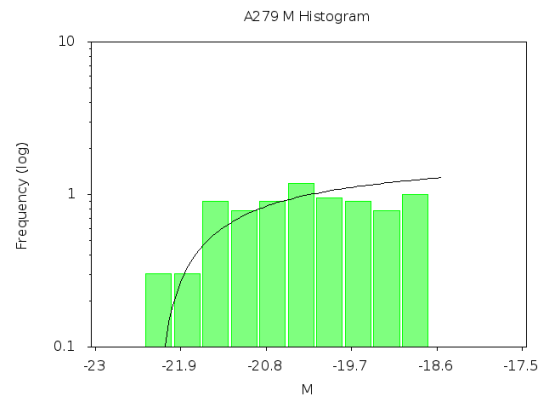
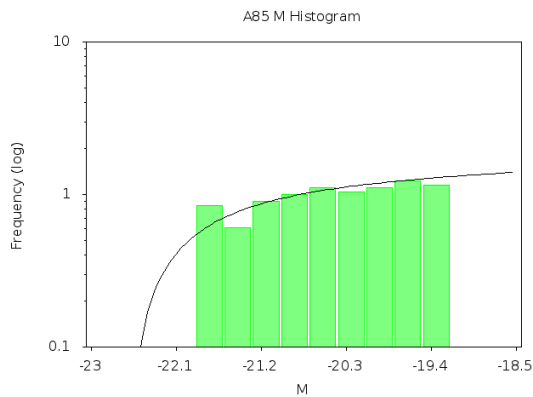


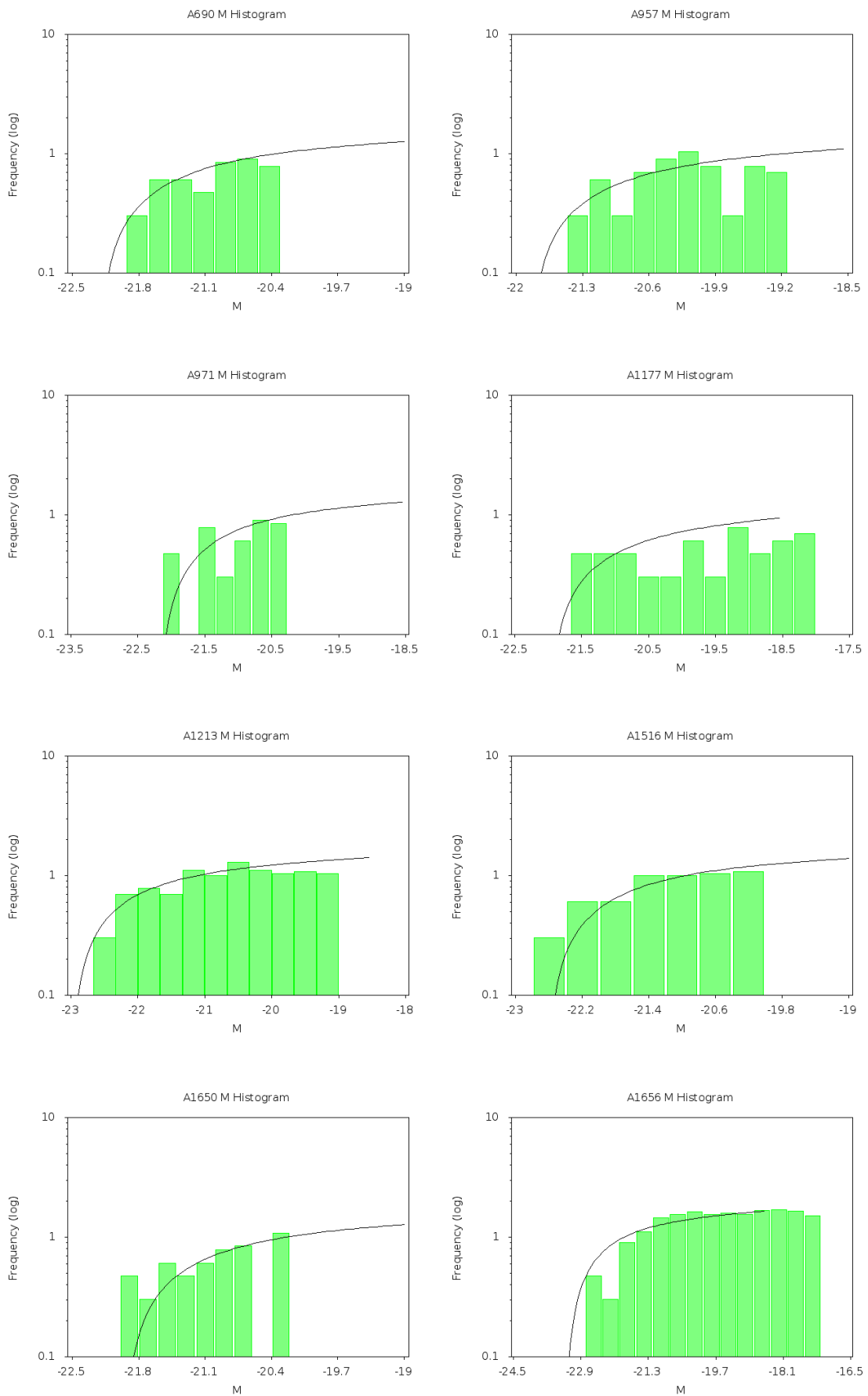


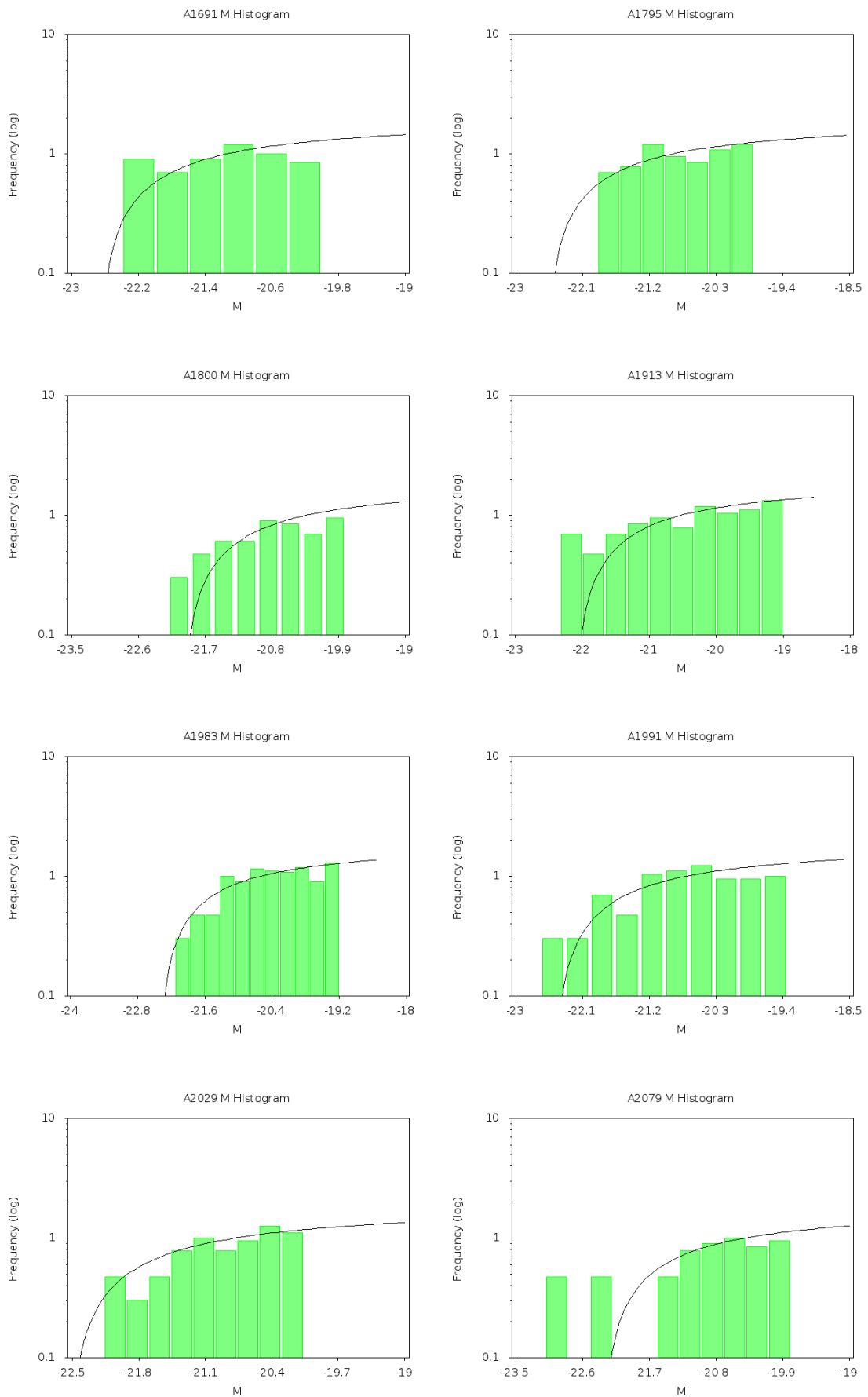
Appendix C

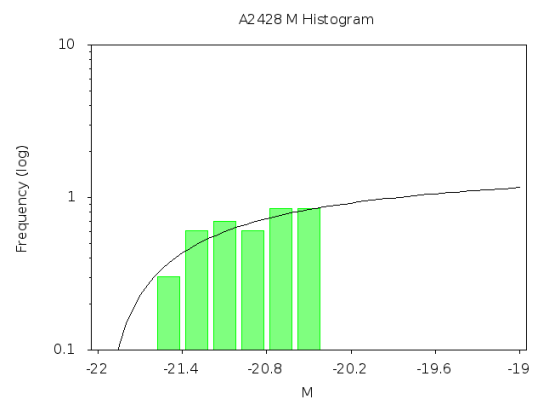
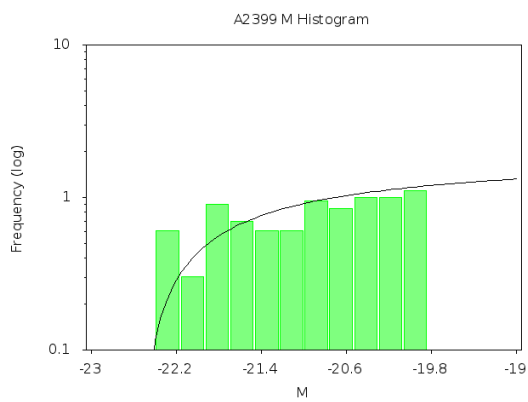
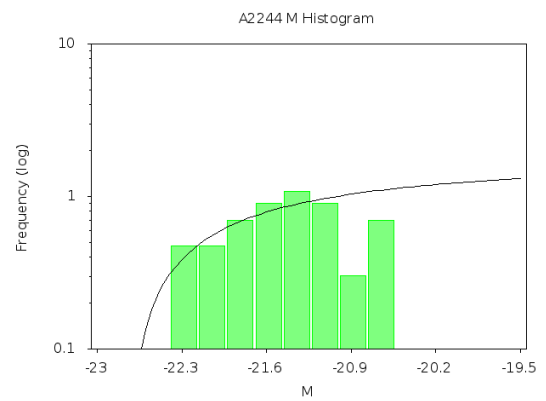
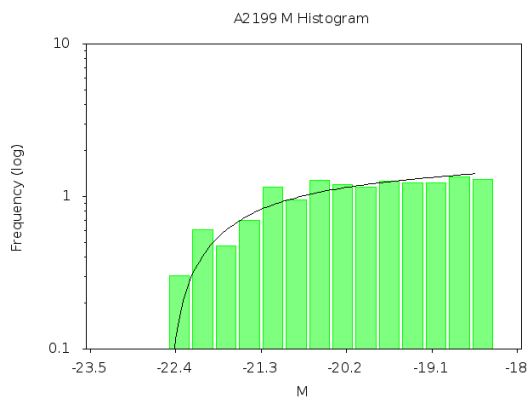
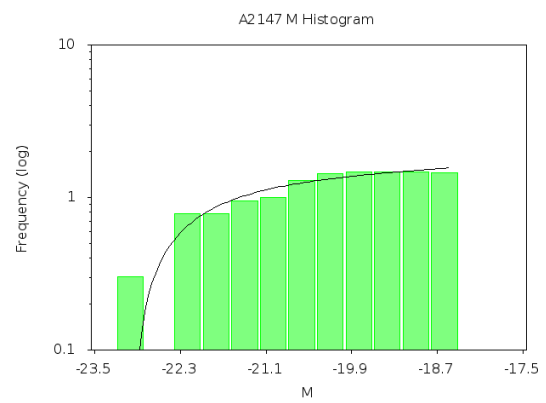
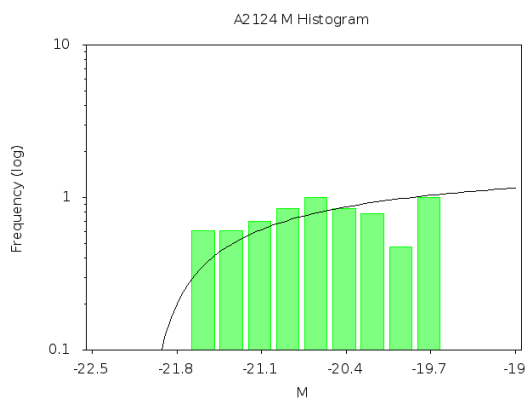
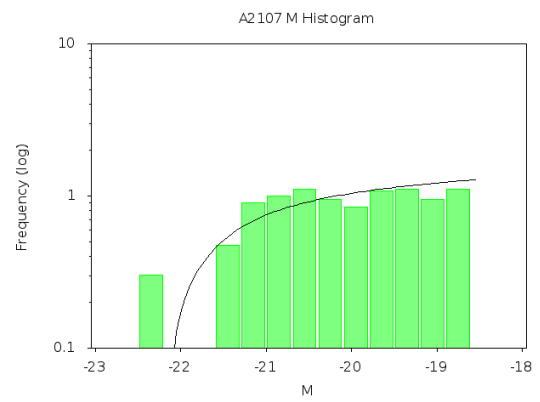
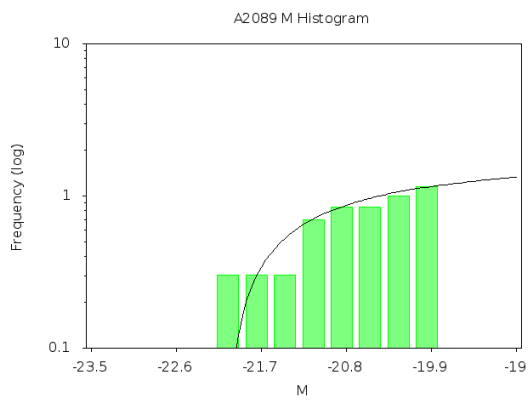
Luminosity Function Diagrams

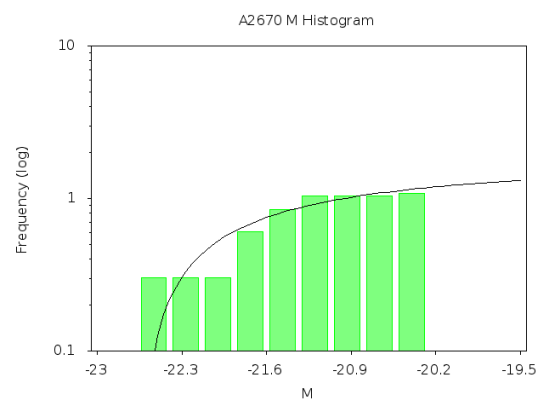
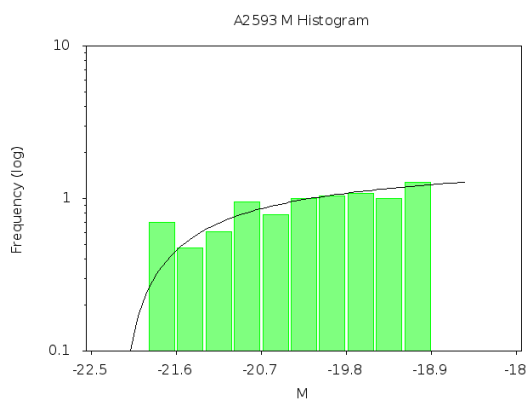
In this Appendix, we present the Luminosity Function Diagrams for each of our Abell clusters. The diagrams presents histograms of galaxy absolute magnitudes for each cluster, along with the best-fit Schechter function in each case. It is worth noting that the procedure described was not followed for the small number of clusters that consisted of multiple subgroups of galaxies.











Bibliography

- [1] van de Weygaert. Observations and morphology of the cosmic web. In *A pan-chromatic View of the clusters of galaxies and the large-scale structure*, page 409. Springer, 2008.
- [2] S.Borgani. Cosmology with clusters of galaxies. In *A pan-chromatic View of the clusters of galaxies and the large-scale structure*, page 287. Springer, 2008.
- [3] Sarazin. Gas dynamics in Clusters of galaxies. In *A pan-chromatic View of the clusters of galaxies and the large-scale structure*, page 1. Springer, 2008.
- [4] Planck Collaboration: Ade et al. Planck 2013 results. XVI. cosmological parameters. *Astronomy and Astrophysics*, 571:16, 2014.
- [5] Bahcall. *Formation of Structure in the Universe*. Cambridge University Press, 1999.
- [6] Carlberg et al. Ω_m and the CNOC Surveys. 1997.
- [7] Girardi et al. Optical luminosities and mass-to-light ratios of nearby galaxy clusters. *ApJ* 62, 530:62, 2000.
- [8] Kravtsov. The size-virial radius relation of galaxies. *ApJ*, 764,L31, 2012.
- [9] Andernach et al. The cluster m/l ratio and the value of Ω_m . *Astronomical Society of the Pacific Conference Series*, 329:289–293, 2005.
- [10] Bravo-Alfaro et al. Galaxy evolution in Abell 85. *Astronomy and Astrophysics*, 495:379–387, 2009.
- [11] Carlberg et al. Galaxy cluster virial masses and . *ApJ*, 462:32–49, 1996.
- [12] Mahdavi et al. Evidence for non-hydrostatic gas from the cluster x-ray to lensing mass ratio. *MNRAS*, 384:1567–1574, 2007.
- [13] Montero-Dorta et al. The SDSS DR6 luminosity functions of galaxies. *MNRAS*, Volume 399:1106–1118, 2008.

-
- [14] Barkhouse et al. The luminosity function of low-redshift abell galaxy clusters. *ApJ*, 671:1471–1496, 2007.
- [15] Hansen et al. Measurement of galaxy cluster sizes radial profiles and luminosity functions from sdss photometric data. *ApJ*, 633:122–137, 2005.
- [16] Plionis et al. Mass-to-light ratios and the value of the density parameter ω_m . *Lecture Notes in Physics*, 592:147, 2005.
- [17] Maurogordato et al. A sample of galaxy clusters to study the fundamental plane:redshift measurements. *Astronomy and Astrophysics Supplement series, Vol. 123, Jun II 1997, 411-422.*, 123:411–422, 1997.
- [18] Popesso et al. A unified picture of the cluster luminosity function. *Astronomy and Astrophysics*, 433:415–429, 2005.